T2R2 東京科学大学 リサーチリポジトリ
Science Tokyo Research Repository

論文 / 著書情報
Article / Book Information

題目(和文)	
Title(English)	Study on Thin Film Transistors using Liquid Crystalline Organic Semiconductor and Silver Electrodes
著者(和文)	KangSabina
Author(English)	Sabina Kang
出典(和文)	学位:博士(工学), 学位授与機関:東京工業大学, 報告番号:甲第12619号, 授与年月日:2023年12月31日, 学位の種別:課程博士, 審査員:飯野 裕明,梶川 浩太郎,間中 孝彰,大見 俊一郎,田口 大,長谷川 達生
Citation(English)	Degree:Doctor (Engineering), Conferring organization: Tokyo Institute of Technology, Report number:甲第12619号, Conferred date:2023/12/31, Degree Type:Course doctor, Examiner:,,,,,
学位種別(和文)	博士論文
Type(English)	Doctoral Thesis

Powered by T2R2 (Science Tokyo Research Repository)

東京工業大学
Tokyo Institute of Technology

Study on Thin Film Transistors using Liquid Crystalline Organic Semiconductor and Silver Electrodes

Sabina Kang

Supervisor: Associate Professor Hiroaki Iino

Electrical and Electronic Department

Graduate School of Engineering

Tokyo Institute of Technology

TABLE OF CONTENTS

Chapter 1

Introduction

1.1 Organic electronics

Organic electronics have attracted notable attention due to their potential applications for large-area manufacturing, flexibility, and low-temperature and low-cost fabrication such as the printing process [1]–[7] Nowadays, semiconductors based on silicon have widely applied to electronics and become an indispensable essential part of our life, however, limited by their resources and methodologies silicon electronics have challenges in low-cost and environment-friendly manufacture. Therefore, these organic materials possess unique properties making them an attractive alternative to conventional electronics. Organic electronics can be allowed the processing under low temperatures and solution processes, such as printing techniques so that can realize low-cost manufacturing. Also, its mechanical flexibility and compatibility which can be easily integrated onto unconventional substrates, like plastic or fabric with plastic substrates enables the application of bendable and stretchable electronics which the needs have notably increased recently, such as curved or foldable displays. Moreover, its feature of biocompatibility with flexibility opens up new avenues for the development of wearable technology, electronic textiles, and conformal electronics for healthcare applications. Last, the lightweightness accelerates the practical application of wearable electronics on a large scale.

1.2 Liquid crystalline organic semiconductors

1.2.1 Aggregation state of organic semiconductors

Amorphous organic semiconductors exhibit low mobility, but it has an advantage to fabrication uniform film in a large area. On the other hand, crystal materials show high mobility, but it is difficult to achieve uniformity in a large area. Liquid crystal state is a mesomorphic state, or liquid crystal phase, whose physical properties are between those of conventional isotropic liquids and those of conventional crystal solids as shown in Fig. 1.1. In addition to the high mobility that is 10^2 to 10^3 times higher than those of amorphous organic films, liquid crystals exhibit several unique features attributed to their soft-nature and self-organization that distinguish them from non-liquid crystalline materials[8]–[10]. Therefore, liquid crystal material will be realized for high performance in electronic devices and easy process for device fabrication.

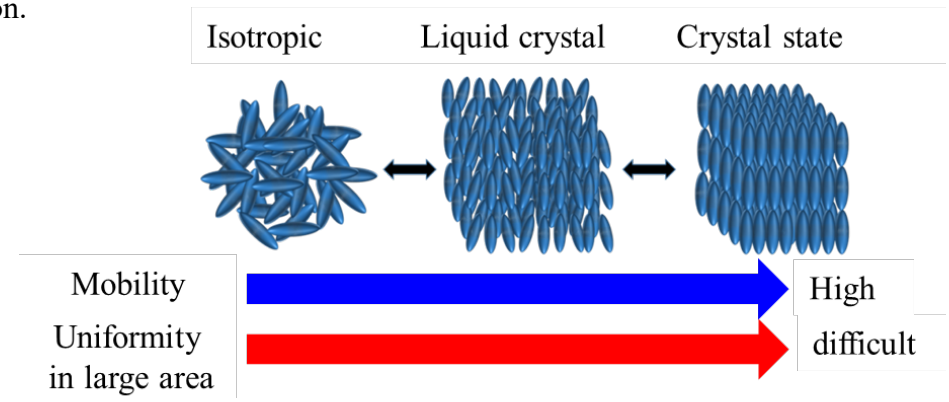

Figure 1.1 Schematic diagram appearance of the liquid crystal state in a temperature profile, with a correlation between material state and mobility and uniformity in a large area.

1.2.3 Advantages of liquid crystals for organic electronics

Smectic liquid crystals show a soft nature compared with crystalline materials due to their self-organized manner, and high solubility in organic solvents because of their long side chains. These properties are useful for the solution process of thin films. Furthermore, molecules in the resulting liquid crystalline films tend to form a homeotropic orientation on a substrate in a

self-organized manner due to their anisotropic molecular structure. Such oriented liquid crystalline films are easily transformed to crystalline films with the preserve of ordered structure just by cooling them down to their crystallization temperature. (Fig. 1.2) Therefore, liquid crystalline films can be utilized as a precursor film for crystalline films [9], [11], [12].

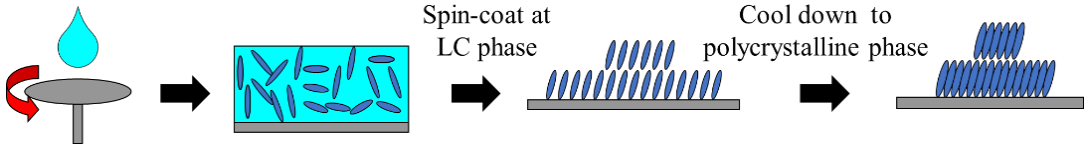

Figure 1.2 Illustration of fabricate polycrystalline thin films from liquid crystal phase

1.2.4 Ph-BTBT-10

Recently developed polycrystalline thin film by small molecular 2-decyl-7-phenyl-[1]benzothieno[3,2-b][1]benzothiophene (Ph-BTBT-10, Fig. 1.3.(a)) is a highly ordered liquid crystal phase, i.e., SmE phase, smectic liquid crystalline materials with asymmetrical substituted the BTBT core with one phenyl and one alkyl chain groups. [11], [13][13, 14] By setting the spin-coating temperature at a SmE temperature, it is utilized the liquid crystal temperature spin-coating method, uniform polycrystalline thin-film without crack can be obtained. In addition, SmE phase of Ph-BTBT-10 appears over 140°C as shown in Fig.1.3(b). It ensures the highly ordered SmE polycrystalline thin film can be maintained over 140°C, and it takes advantage to utilize to transistors in terms of durability.

(a)

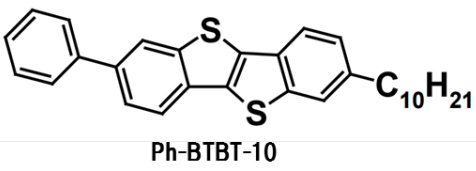

Ph-BTBT-10

(b)

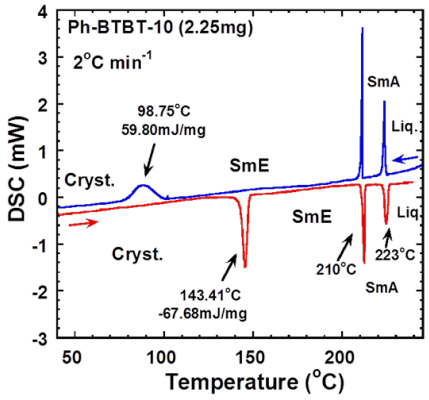

Figure 1.3 (a) Chemical structure of Ph-BTBT-10. (b) Differential scanning calorimetry (DSC) thermogram of Ph-BTBT-10

For the OFET using Ph-BTBT-10, the previous research reported that OFETs performance is dramatically improved by the thermal annealing process. Thermal annealing promotes a change in the step structure from monolayer steps of 2.8 nm, which coincides with the molecule size of Ph-BTBT-10, to bilayer steps of 5.7 nm. Furthermore, the XRD patterns exhibit a distinct change in the peaks at 3.4° and 1.7° before and after thermal annealing, as shown in Fig. 1.4(a). These variations suggest that the monolayer structure with a thickness of 26 Å before thermal annealing was transformed into a bilayer structure with a thickness of 52 Å, as shown in the schematic illustration in Fig. 1.4(a). By this transition of structure, the transport path probably increases (Fig. 1.4 (b)) [13, 14].

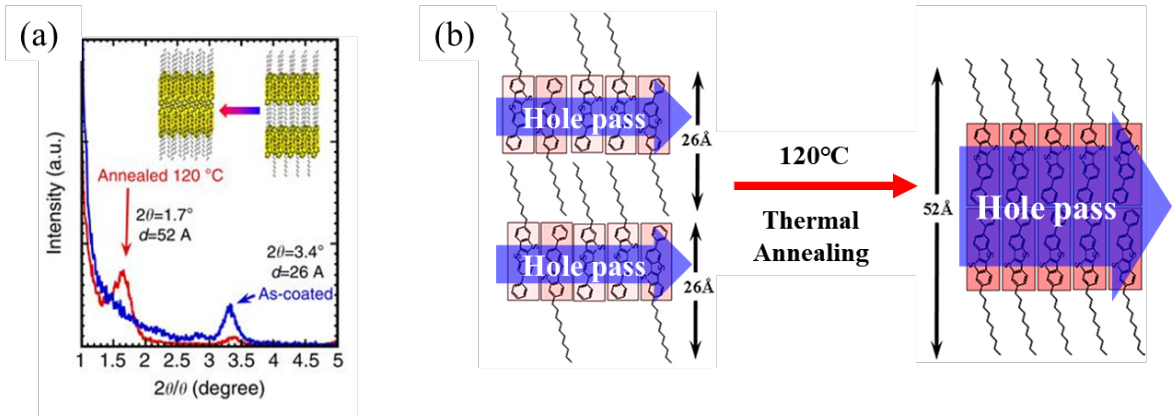

Figure 1.4 (a) XRD patterns for crystalline films as-coated and after annealing, with a schematic illustration of the crystalline structure (b) Schematic illustration of transport path as-coated and after annealing.

1.3 Silver electrodes

Most reports of high-performance OFETs with Ph-BTBT-10 used gold source-drain (S/D) electrodes due to their high conductivities, and ability to form excellent contact with most p-type organic semiconductors [14]–[16]. Nevertheless, the high cost of gold offsets its practical applications in low-cost electronics. On the other hand, low-cost metal silver can be an effective approach to dramatically reduce the cost, although it shows poor properties compared to gold. Furthermore, by this approach, it is also expected the printing techniques for the fabrication of Ag electrodes such as inkjet printing, screen printing, and offset printing.

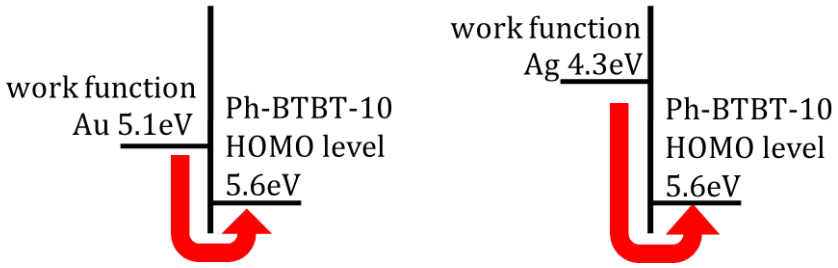

Figure 1.5 Schematic illustration of energy level diagram of Au/Ph-BTBT-10 interface and Ag/Ph-BTBT-10 interface.

1.3.1 Vacuum-deposited silver electrodes

Physical vapor deposition (PVD) techniques deposit thin films, in which a target material is vaporized and transported on the substrate in a vacuum. PVD techniques include sputtering, electron beam (EB), and thermal evaporation, and in this study, thermal and EB evaporation were used to fabricate silver S/D electrodes. Both thermal and EB vacuum-depositions have featured that atomic deposition from the vapor, in-situ control of the evaporated layer thickness which leads to small thicknesses, and estimations of film thickness uniformity. However, these require high temperatures and high vacuum conditions, it does not match the need for next-generation organic electronics that demand environmentally friendly and low-cost

manufacturing.

1.3.2 Solution-processed silver electrodes

Compared with conventional dry process in a vacuum, fabrication processes based on solution process are expected to provide large-area, and low-cost manufacturing by printing and roll to roll process. Therefore, the solution process is realizing printed electronic devices, such as organic field-effect transistors [17], [18] [18-20] and flexible displays , [21]. Many research groups have investigated to improve the performance of organic thin-film transistors with printed electrodes. In their researches, printing methods were used for patterning the S/D electrodes; for example, channel lengths around 10 μm were realized by inkjet printing, [22, 23] and, channel lengths of 30 and ～60 μm were realized by screen printing. [24] However, with the above printing methods it is difficult to get fine pattern by only printing technique, some research groups have suggested printing methods with the difference in surface wettability in order to fabricate fine patterns. [25] Also, other research groups have fabricated fine patterning silver nanoparticle electrodes by hydrophobic/hydrophilic patterning of a substrate surface by spin coating process [26]. In this study, also, solution-processed silver electrodes have been investigated.

1.4 Interfacing engineering

The interface between S/D electrode and organic semiconductor is important in OFETs, which determines the carrier injection property. In an ideal OFET, ohmic contact is assumed, and the contact resistance is much lower than the channel resistance. [15] However, Schottky contact and injection barrier are usually present in real OFETs and leads to large contact resistance. Focusing on OFETs with silver electrodes, OFETs with silver electrodes have bigger energy mismatch between the work function of silver electrode and the highest occupied molecular orbital (HOMO) level of Ph-BTBT-10 than those with gold electrodes (Fig. 1.6). This energetic misalignment causes a high hole-injection barrier and high contact resistance. Therefore, the carrier injection barrier, which is determined by the work function of the electrodes and the HOMO level of the organic semiconductors, is an important parameter and it is important to evaluate the electrode/organic layer interface. The modification of the electrode by a self assembled monolayer (SAM) occur the energy shift at the metal and organic semiconductor interface by the interface dipole of SAM molecule. As shown in Fig. 1.6(a), the direction of the interface dipole of SAM molecules controls the direction of the energy level shift. The hole barrier height is reduced when the interface dipole is directed form the organic semiconductor to the metal. Pentafluorobenzenethiol (PFBT), whose chemical structure shown in Fig. 1. 6 (b), is known to contain strong electron-withdrawing group in fluorinated benzene part. [27-29].

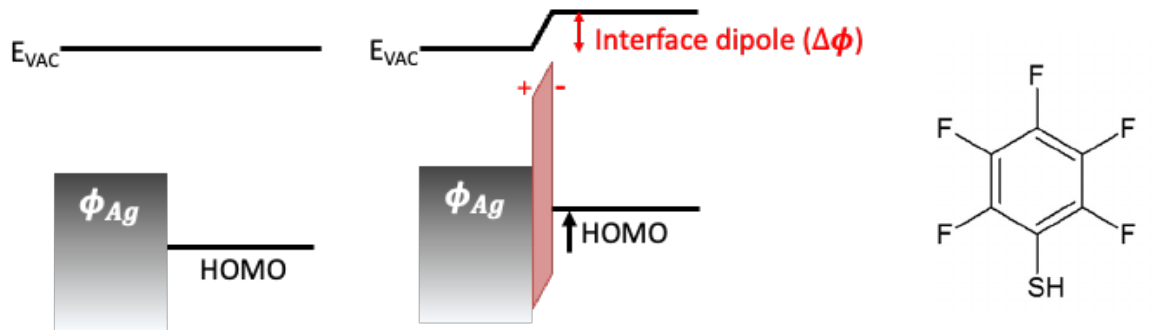

Figure 1.6 (a) Schematic illustration of energy level shift induced by SAMs treatment. (b) Chemical structure of PFBT. ϕ_{Ag}: is he work function of pristine Ag and $\Delta\phi$ is potential across dipole layer

1.6 Objective and content of this study

Therefore, this study focuses on the fabrication of high-performance low-cost OFETs with liquid crystalline organic semiconductor Ph-BTBT-10 using the silver S/D electrodes as different device structures and fabrication methods.

This study consists of six chapters. Chapter 1 introduces the background, motivation, and aims of this study. Chapter 2 describes the experimental methods of this study. In chapter 3 and 4, Ph-BTBT-10 thin film transistor using silver S/D electrodes were investigated as different OFETs structure top contact and bottom contact, respectively. In chapter 5, solution processed silver electrodes will be demonstrated. In the last chapter, chapter 6, the final conclusion of this study was made, then prospective was given.

References

[1] A. Sandström, H. F. Dam, F. C. Krebs and L. Edman, "Ambient fabrication of flexible and large-area organic light-emitting devices using slot-die coating," Nat Commun, vol. 3, no. 1002, 2012.

[2] C. Lungenschmied, G. Dennler, H. Neugebauer, S. N. Sariciftci, M. Glatthaar, T. Meyer and A. Meyer, "Flexible, long-lived, large-area, organic solar cells," Solar Energy Materials and Solar Cells, vol. 91, no. 5, pp. 379-384, 2007.

[3] Dimitrakopoulos, C.D. and Malenfant, P.R., Organic thin film transistors for large area electronics. Adv. Mater. **14** (2), 99-117 (2002).

[4] M. R. Niazi, R. Li, E. Q. Li, A. R. Kirmani, M. Abdelsamie, Q. Wang, W. Pan, M. M. Payne, J. E. Anthony, D.-M. Smilgies, S. T. Thoroddsen, E. P. Giannelis and A. Amassian, "Solution-printed organic semiconductor blends exhibiting transport properties on par with single crystals," Nat Commun, vol. 6, no. 8598, 2015.

[5] A. Pierre, I. Deckman, P. B. Lechêne and A. C. Arias, "High Detectivity All-Printed Organic Photodiodes," Adv. Mater., vol. 27, pp. 6411-6417, 2015.

[6] H. Shirakawa, E. J. Louis, A. G. MacDiarmid, C. K. Chiang, A. J. Heeger, J. Chem. Soc. Chem. Comm, 578 (1977).

[7] A. J. Heeger, Chem. Soc. Rev, **39**, 2354 (2010).

[8] A. Tsumura, H. Koezuka, T. Ando, Appl. Phys. Lett. **49**, 1210 (1986).

[9] H. Li , B. C. K. Tee , J. J. Cha , Y. Cui , J. W. Chung , S. Y. Lee , Z. Bao , J. Am. Chem. Soc. **134**, 2760 (2012).

[10] Jun-ichi, and Hiroaki IINO. "Liquid Crystals as an Organic Semiconductor for Printed Electronics." NIHON GAZO GAKKAISHI (Journal of the Imaging Society of Japan) 51.5 (2012): 531-536.

[11] T. Kato, N. Mizoshita, K. Kishimoto, Angew. Chem. Int. Ed, **45**, 38-68 (2006).

[12] R. J. Bushby, S.M. Kelly, M. O'Neill (Eds), Liquid Crystalline Semiconductors:

[13] Iino, H., Usui, T. and Hanna, J.I., Liquid crystals for organic thin-film transistors, Nat, commun. **6** (1), 1-8 (2015).

[14] Iino, H. and Hanna, J.I., Liquid crystalline organic semiconductors for organic transistor applications, Polym. J. **49** (1), 23-30 (2017).

[15] Di, Chong-An, et al., Interface engineering: an effective approach toward high-performance organic field-effect transistors, Acc. Chem. Res. **42**(10), 1573-1583, (2009)

[16] Kim, C.H. *et al*., Decoupling the effects of self-assembled monolayers on gold, silver, and copper organic transistor contacts, *Adv. Mater. Interfaces* **2** (2), 1400384 (2015).

[17] Chung, S. et al., Contact resistance of inkjet-printed silver source–drain electrodes in bottom-contact OTFTs, J. Disp. Technol. **8** (1), 48-53 (2011).

[18] Minemawari H., Yamada T., Matsui H., Tsutsumi J., Haas S., Chiba R., Kumai R. and Hasegawa T. 2011 Nature **475** 364

[19] Teichler A., Eckardt R., Hoeppener S., Friebe C., Perelaer J., Senes A., Morana M., Brabec C. J. and Schubert U. S. 2011 Adv. Energy Mater. **1** 105

[20] Kumaki D., Fujisaki Y. and Tokito S. 2013 Org. Electron. **14** 475

[21] Fukuda K., Sekitani T., Zschieschang U., Klauk H., Kuribara K., Yokota T., Sugino T., Asaka K., Ikeda M., Kuwabara H., Yamamoto T., Takimiya K., Fukushima T., Aida T., Takamiya M., Sakurai T. and Someya T. 2011 Adv. Funct. Mater. **21** 4019

[22] Fukuda K., Hikichi K., Sekine T., Takeda Y., Minamiki T., Kumaki D. and Tokito S. 2013 Sci. Rep. **3** 2048

[23] Chung S., Jeong J., Kim D., Park Y., Lee C. and Hong Y. 2012 J. Disp. Technol. **8** 48

[24] Lim S. C., Kim S. H., Yang Y. S., Lee M. Y., Nam S. Y. and Ko J. B. 2009 Jpn. J. Appl. Phys. **48** 081503

[25] Sirringhaus H., Kawase T., Friend R. H., Shimoda T., Inbasekaran M., Wu W. and Woo E. P. 2000 Science **290** 2123

[26] Sugano, R., Takeda, Y., Kobayashi, Y., Fukuda, K., Kumaki, D., & Tokito, S. (2014). Fine patterning method for silver nanoparticle electrodes using differential hydrophobic and hydrophilic surface properties. Japanese Journal of Applied Physics, 53(4S), 04EK01.

[27] Love, J.C. et al., Self-assembled monolayers of thiolates on metals as a form of nanotech nology, Chem. Rev. **105** (4), 1103-1170 (2005).

[28] Kim, H. et al., Large enhancement of hole injection in pentacene by modification of gold with conjugated self-assembled monolayers, Org. Electron. **14** (9), 2108-2113 (2013).

[29] Khodabakhsh, S., Poplavskyy, D., Heutz, S., Nelson, J., Bradley, D.D., Murata, H. and Jo nes, T.S., 2004. Using self-assembling dipole molecules to improve hole injection in conj ugated polymers. Advanced Functional Materials, 14(12), pp.1205-1210.

Chapter 2

Experimental methods

2.1 Materials

2.1.1 Liquid crystalline organic semiconductor materials

2-Decyl-7-phenyl-[1]benzothieno[3,2-b][1]benzothiophene (Ph-BTBT-10) [1], [2] which is one of the liquid crystalline organic semiconductor material was used for the semiconductor layer of the OFETs.

2.1.2 Substrates

In this study, heavily doped silicon wafers with a silicon dioxide (SiO_2) dielectric layer, a thickness of 300 nm, were used in fabricating OFETs, except for photo patterning OFETs. Most OFETs were prepared with the silicon wafer cut into lengths of 20 mm × 25 mm.

2.1.3 Electrodes materials

In order to compare the performances of OFETs with silver source/drain (S/D) electrodes and those with gold S/D electrodes, both silver and gold metals were prepared and vacuum deposited.

2.1.4 Silver nanoparticles

In this study, two kinds of silver nanoparticle ink were used for the fabrication of solution-processed silver S/D electrodes. One of the silver nanoparticle ink was provided

by Harima Chemicals, Inc. (NPS-L) [3]. It is dispersed in the hydrocarbon organic solvent, tetradecane. The other silver nanoparticle ink is dispersed in glycerin and water, which has more hydrophilic properties than organic solvents. It was synthesized and provided by Bando Chemical Industries, Ltd.

2.1.5 Photoreactive self-assembled monolayers

To pattern silver S/D electrodes by solution process, photoreactive self-assembled monolayers (SAM) were used, provided by Nikon Corporation [4]. The photoreactive SAM is composed of a photo-responsive part and an adhesion part. Also, the photo-responsive part is divided into a protective group and protected amino as shown in Fig. 2.1. A fluorinated functional group is introduced to this protective group, which is in R of molecular structure. Therefore, the photoreactive SAM-treated substrates have hydrophobic properties. As the substrates are exposed to UV, the protective group is decomposed and eliminated, and then the amino group, which has hydrophilic properties, appears. Consequently, silver nanoparticles can be selectively patterned due to the differential surface energy of hydrophobic and hydrophilic.

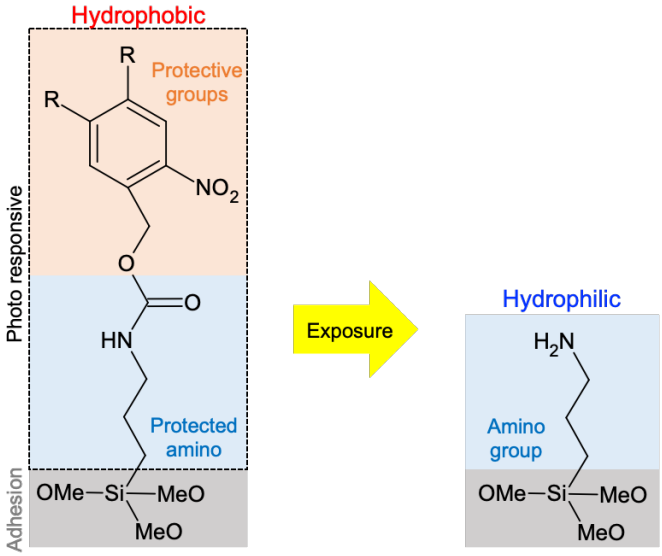

Figure 2.1 Molecular structure of photoreactive self-assembled monolayer before and after the photoreaction.

2.2 Fabrication method

2.2.1. Structure of OFETs

In this study, two kinds of OFET structures are used, the bottom-gate top-contact configuration OFETs and the bottom-gate bottom-contact configuration OFETs as shown in Fig. 2.2. Si/SiO_2 substrates were prepared, so silicon was used as gate electrodes and silicon dioxide was used as the dielectric layer.

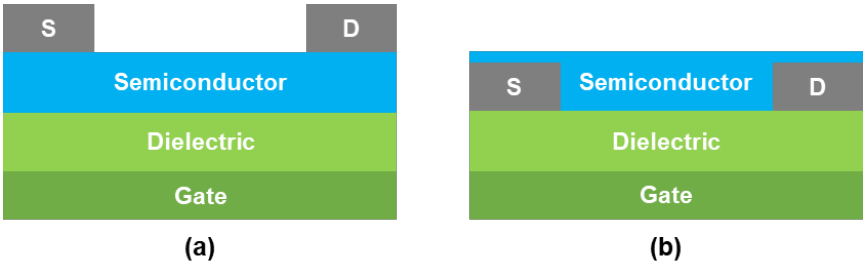

Figure 2.2 Schematic illustration of organic field-effect transistor structures. (a) Bottom-gate top-contact. (b) Bottom-gate bottom-contact.

2.2.2 Substrate cleaning

All Si/SiO_2 substrates were cleaned according to the following procedure and conditions:

1. Ultrapure water with neutral detergent by an ultrasonic cleaner for 5 minutes.
2. Rinse with ultrapure water 5 times.
3. Ultrapure water by an ultrasonic cleaner for 5 minutes twice.
4. Isopropyl alcohol (IPA) by ultrasonic cleaner for 5 minutes.
5. Acetone by ultrasonic cleanser for 5 minutes.
6. IPA by ultrasonic cleaner for 5 minutes.
7. Heat with acetone on the hot plate at 130 °C
8. Dry Si/SiO_2 substrates on the hot plate.

2.2.3 Ph-BTBT-10 thin film by spin coating

Spin coating is a solution process used to deposit uniform thin films onto flat substrates. It has the advantage that a uniform thin film can be easily obtained under the atmosphere conditions without a vacuum deposition process. General operation is first dropping a small amount of solution on the center of the substrate. The substrate is then rotated at high speed to spread the coating material by centrifugal force. In this study, so as to spin coat at liquid crystal phase temperature, Ph-BTBT-10 solution, Si/SiO_2 substrates, and Pasteur pipette were heated on a hot plate. Also, it is difficult to control the temperature when the substrate is moved from the hot plate to the stage of the spin-coater, so to increase the heat capacity, the glass substrates have adhered under the Si/SiO_2 substrates with double-sided tape to prevent temperature decrease quickly. Also, to reduce the variation affected by the solution temperature, the temperature was monitored with an infrared thermometer, as shown in Fig. 2.3. After Ph-BTBT-10 solution was dropped on the substrate, the spin coater was operated at the temperature when the temperature of infrared thermometer was at 69~70 ℃, which means that calibrated temperature is 90 ℃ and supercooled liquid crystal phase temperature [1], [2]. The spin coat condition in this study:

1. Ph-BTBT-10 thin films, 0.45wt%, p-Xylene solution at the liquid crystal phase temperature of 110 ℃ and cooling the liquid crystal films to room temperature.

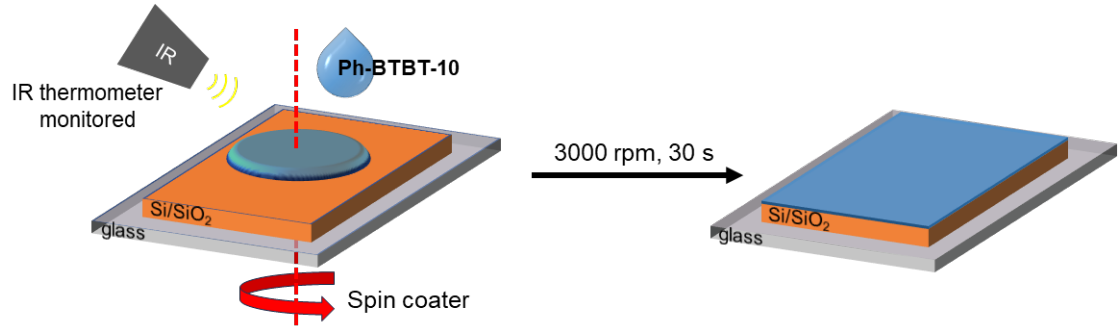

Figure 2.3 Schematic illustration of spin coating process for liquid crystalline organic semiconductors

2. The hot plate heating temperature was usually 170°C, however, it was controlled a little bit depending on the season, and the number of substrates on the stage.

3. The spin speed and time were 3000 rpm and 30 seconds, respectively.

2.2.4 Thermal Annealing

After spin-coating Ph-BTBT-10 thin film, the substrates were thermally annealed. In the previous research [5], the optimum condition for annealing temperature and time was investigated and it suggested a temperature of 120℃ for 15 minutes for thermal annealing of Ph-BTBT-10 thin film. Therefore, all devices fabricated in this thesis applied this condition. In the experiment, the petri dish which is used to put the devices into the oven was preheated to prevent temperature variations.

2.2.5 Fabrication of electrodes using vapor deposition

S/D electrodes were vacuum deposited by either the thermal evaporator or the electron beam evaporator. For the top-contact configuration OFETs, both silver and gold S/D electrodes were fabricated with a thickness of 30 nm on Ph-BTBT-10 thin film. For the bottom-contact configuration OFETs, the thickness of gold S/D electrodes was fabricated at 30 nm on Si/SiO_2 substrates, whereas the thickness of silver S/D electrodes was given the variation from 30 nm to 70 nm to improve the carrier injection, and the details and results are explained in Chapter 4.

2.2.6 Fabrication of electrodes using solution processes

Various solution-processed silver S/D electrode patterning methods are handled which is ink-jet printing and methods utilizing properties of hydrophobic and hydrophilic based

on the differential surface energy with a couple of concepts: hydrophobic and hydrophilic SAMs, fluorine-polymer (CYTOP: provided by AGC Inc.) layer with O_2 plasma; photoreactive SAM [4]. As a method of photo-patterning without using a resist, photo-responsive surface treatment substrates were used. In this method, fine electrodes pattern could be fabricated with metal. Each concept will be described in detail in Chapter 5.

2.2.7 Self-assembled monolayers treatment

In order to ensure good electrical contact between Ph-BTBT-10 thin film and S/D electrodes in the bottom-gate bottom-contact configuration, S/D electrodes were modified with self-assembled monolayers (SAMs): pentafluorobenzenethiol (PFBT), 4-(trifluoromethyl)-benzenethiol (TFBT) and 2,3,5,6-tetrafluoro-4-(trifluoromethyl)-Benzenethiol (TTFP), purchased from Tokyo Chemical Industry Co., Ltd. SAMs treatment of the S/D electrodes was conducted by immersing the substrate in dehydrated ethanol solution of PFBT in the glove box. The SAM-treated S/D electrodes were then removed from the solution and rinsed with ethanol. For the gold electrodes, conventional SAMs treatment condition carried out our laboratory is 100 mM dehydrated ethanol solution of PFBT. In this thesis the concentration of PFBT solution was discussed. Furthermore, to reduce of process time and simplify of process steps, vapor process was considered. It was conducted under ambient-pressure vapor deposition at 100 °C for 15 mins capping with a petri dish.

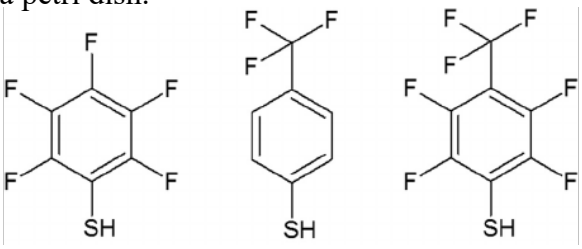

Figure 2.4 Chemical structure of (a) pentafluorobenzenethiol (PFBT), (b) 4-(trifluoromethyl)-benzenethiol (TFBT), and (c) 2,3,5,6-tetrafluoro-4-(trifluoromethyl)-benzenethiol (TTFP)

2.3 Evaluation method

2.3.1 Optical microscopy

Surface morphology of polycrystalline thin films in macro scale was observed under optical microscopy (Nikon corporation) with reflection mode. The uniformity of film was judging from the color pattern of texture. A uniform film will give same color in whole area under the scope, while the bare substrate gives a color in purple.

2.3.2 Measurement of OFET performance

The OFETs performance was characterized by two source measurement units (8252, ADCMT) under the ambient condition at room temperature. The mobility (μ) was calculated by plotting the square root of the source-drain current (I_{ds}) versus gate voltage (V_g) using the equations below:

$$I_{ds} = C_i \frac{W}{L} \mu \left(V_g - V_{th}\right) V_{ds} \quad \text{(In linear region)}$$

$$I_{ds} = C_i \frac{W}{2L} \mu \left(V_g - V_{th}\right)^2 \quad \text{(In saturated region)}$$

where C_i is capacitance of gate insulator and V_{th} is threshold voltage.

2.3.3 Transfer length method

In order to analyze contact resistance, the transfer length method (TLM) analysis was used. Since total resistance (R_{total}) of the on-state OFET operated in linear regime can be expressed as a summation of channel resistance ($R_{channel}$) and contact resistance (R_c), the contact resistance can be extracted by using the following equations:

$$R_{total} = R_{ch} + R_C$$

$$R_{total} \times W = \frac{L}{\mu C_i (V_g - V_{th})} + R_C \times W$$

where W, L, μ, C_i, V_g, and V_{th} are channel width, channel length, mobility, channel capacitance per unit area, gate voltage, and threshold voltage, respectively. From the above equation, R_c can be extracted from a linear plot of R_{total} versus different channel lengths for various gate voltages, by obtaining the intersection with the y-axis.

2.3.4 Photoemission spectroscopy in air

Photoelectron yield spectroscopy in air (PYSA), AC-3 of RIKEN keiki corporation, was used to measure the work function of metal electrodes and the ionized potential of Ph-BTBT-10. Monochromatic light is incident on the sample controlling photon energy to increase. When the photon energy exceeds the work function of the samples, photoemission occurs. And then these emitted photoelectrons are counted. The x-axis represents the energy of the incident UV photoelectrons, and the y-axis represents the photoelectron yield. This threshold energy, as shown in Fig. 2.5, can be interpreted as a work function or ionization potential. For the samples, Ph-BTBT-10 was spin-coated on Si/SiO_2 substrates, and metal electrodes were vacuum-deposited on Si/SiO_2 substrates. Details of fabrication process followed in the former section. The incident photon energy ranges from 4 eV to 6.5 eV.

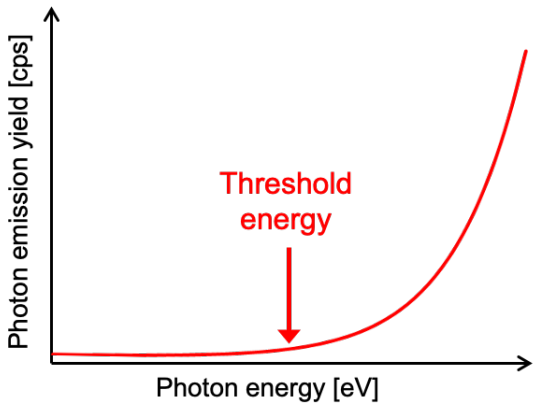

Figure 2.5 Schematic diagram of photoemission spectroscopy spectra

2.3.5 Contact angle

The contact angle (θ) is the angle measured through the liquid where a liquid/vapor interface meets a solid surface. In this thesis, the θ/2 method is used for the measurement of contact angles, following the equation given below: where r is radius and h is height of the droplet, as shown in Fig. 2.6. In addition, the contact angle is obtained from the angle of straight lines connecting the left and right ends and the apex of the droplet against a solid surface.

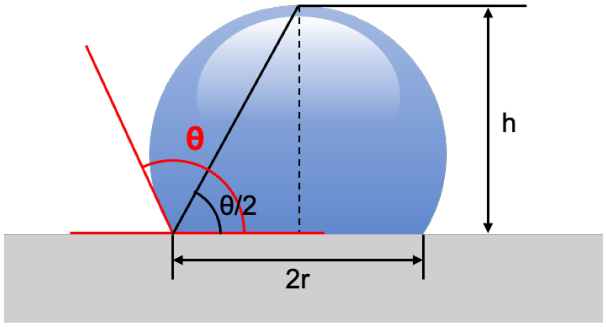

$$\tan\frac{\theta}{2} = \frac{h}{r}$$

$$\theta = 2\tan^{-1}\frac{h}{r}$$

Figure 2.6 Schematic illustration of contact angle measurement.

2.3.6 Time-of-flight secondary ion mass spectrometry

In this study, to observe the interface between the organic semiconductor and the electrode and distribution, Time-of-flight secondary ion mass spectrometry (TOF-SIMS) was observed. TOF-SIMS is used for the surface analysis of a solid sample's elemental and molecular composition and special distribution, by providing mass spectra, 2D surface images, and depth profiling. Primary ion beam (Bin+, Cs+, Ar+, etc.) is irradiated on a solid sample, and mass separation of the ions emitted from the surface (secondary ions) is performed using the difference in time-of-flight. The mass spectrometer measures an ion's mass-to-charge ratio (m/z) by precisely timing how long it takes to reach the detector. Samples were fabricated in bottom-gate top-contact configuration. After spin

coating Ph-BTBT-10, metal electrodes were vacuum deposited by thermal evaporator on the whole film. The thickness of the silver and gold electrodes was 30 nm.

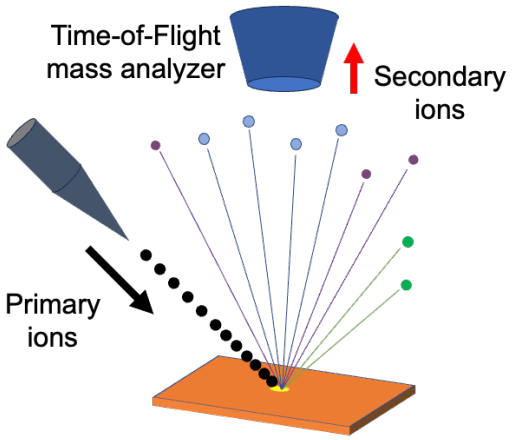

Figure 2.7 Schematic diagram illustrating the fundamental principles of TOF-SIMS.

2.3.7 Scanning electron microscope

Scanning electron microscope (SEM), FE-SEM S-5500 made by Hitachi High-Technologies, Inc., was used to observe the interface between the organic semiconductor and the electrode. SEM is a type of electron microscope that uses a focused beam of high-energy electrons to generate a variety of signals at the surface of solid specimens and is designed for directly studying the surfaces of solid objects. The incident electron beam is scanned over the sample and stimulates the emission of backscattered electrons (BSE) and secondary electrons (SE) from the surface of the specimen. The signals that derive from electron-sample interactions show information about external morphology, chemical composition, and crystalline structure and orientation of materials making up the sample. In most applications, data are collected over a selected area of the surface of the sample, and a 2-dimensional image is generated that displays spatial variations in these properties. So it is suitable for the interface between the organic semiconductor and the electrode that we want to observe in this study. [6] The samples were prepared for

SEM analysis. Each electrode vacuum-deposited on a whole Ph-BTBT-10 layers, and the thickness of silver and gold electrodes were 100 nm and 30 nm, respectively.

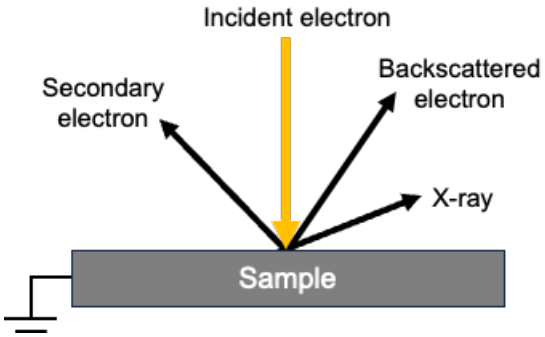

Figure 2.8 Schematic illustration of SEM measurement for sample.

2.3.8 X-ray reflectometry

X-ray reflectometry (XRR) is used to determine thickness, density, and roughness for single and multilayer stacks on substrates. XRR analysis can be performed on both crystalline and amorphous materials. In this study, two different samples were fabricated and compared. One is the silver electrodes were vacuum deposited on the Ph-BTBT-10 layer and then silver electrodes were etched to observe the surface roughness. The other is a pristine Ph-BTBT-10 layer without any treatment. Then, the fitting process was preceded between the measured and the calculated XRR pattern using GlobalFit software, provided by Rigaku Corporation.

References

[1] H. Iino, T. Usui, and J. Hanna, “Liquid crystals for organic thin-film transistors,” *Nat. Commun.*, vol. 6, pp. 6828, Apr. 2015.

[2] H. Iino and J. Hanna, “Availability of liquid crystallinity in solution processing for polycrystalline thin films,” *Adv. Mater.*, vol. 23, no. 15, pp. 1748, Apr. 2011.

[3] M. Ueda, N. Terada, and Y. Matsuba, “Application to the field of electronics of NanoPaste ®,” *The Chemical Society of Japan*, 2019.

[4] Y. Kawakami, “Development of photo responsive material toward fine patterning technology by roll to roll,” *Nikon Research Report (Web)*, vol. 1, pp. 47–52, 2019.

[5] T. Ookura, “Master thesis,” Tokyo Institute of Technology, Mar. 2017.

[6] J. Cho, D. Kim, Y. Jang, W. Lee, K. Ihm, J. Han, S. Chung, and K. Cho, “Effects of metal penetration into organic semiconductors on the electrical properties of organic thin film transistors,” *Appl Phys Lett*, vol. 89, no. 13, Sep. 2006.

Chapter 3
Sutdy on the top contact OFETs using silver S/D elecotrodes

3.1 Introduction

In general, silver electrode is not suitable for p-channel organic transistors because the work function of silver is lower than gold. Indeed, it is reported that the performances of OFETs using silver S/D electrodes are lower than those of gold S/D electrodes in terms of the high contact resistance between organic semiconductors and silver electrodes [1]–[4]. However, since the high cost of gold overshadows practical applications for low-cost electronics, silver can be a promising candidate as electrodes for organic electronics. Generally, it has been demonstrated that the top contact configuration provides better performance compared with that of the bottom one. It is expected that the case of the Ph-BTBT-10 thin-film transistors using silver S/D electrodes also shows better performance compared with the bottom contact configuration. In this chapter, the top contact OFETs using silver S/D electrodes have been investigated and compared to those with gold S/D electrodes.

3.1.1 Fabrication process of top contact OFETs

Figure 3.1 shows the schematic cross-section of Ph-BTBT-10 OFETs with silver S/D electrodes in bottom-gate top-contact configuration. When it comes to the electrodes, to compare the performances of the OFETs with silver S/D electrodes to those with gold S/D electrodes, the experiments were performed on both silver and gold electrodes under the same conditions. Polycrystalline thin films of Ph-BTBT-10 were fabricated by spin coating. After the fabrication of Ph-BTBT-10 thin film, the devices were thermally annealed at 120 ℃ for 15

minutes and by thermal annealing, monolayer crystal structure is transformed into bilayer crystal structure, whose polycrystalline thin films exhibit high mobility [5], [6]. S/D electrodes were deposited on Ph-BTBT-10 thin film by either the thermal evaporator or electron beam evaporator, there were no significant differences between two different evaporators. The deposited thickness of S/D electrodes is 30nm. The details of each step follow the conditions mentioned in Chapter 2.

Figure 3.1 Schematic cross-section of Ph-BTBT-10 thin film transistors used in Chapter 3.

3.1.2 Optical microscopy of Ph-BTBT-10 thin films

OFETs with silver and gold S/D electrodes were fabricated to compare properties. In order to reduce the variations to different conditions such as properties of thin film by spin coating, all substrates were washed, spin-coated, and thermal-annealed at the same time. After that, gold electrodes were vapor-deposited first, and then, silver electrodes did. Figure 3.2(a) and (b) show the optical images of Ph-BTBT-10 thin film with silver and gold electrodes, respectively. It was confirmed that there is no significant difference between OFETs with silver electrodes and those with gold electrodes. The polarized optical microscopy images, which indicate molecular aggregation and alignment, hardly changed and molecular ordering and alignment are not also changed with silver and gold S/D electrodes. (Fig. 3.2(c), (d)) Therefore, it can be concluded that the conditions except for S/D electrode metal are the same.

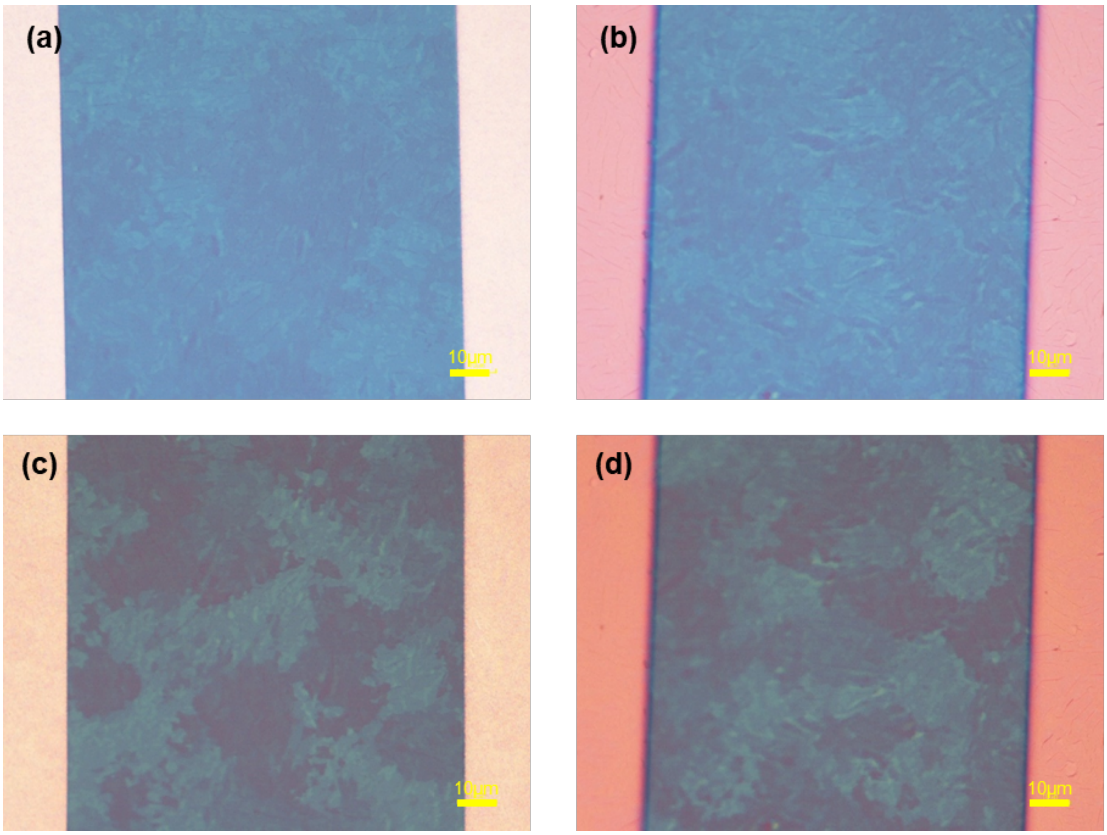

Figure 3.2 Optical microscope images of Ph-BTBT-10 thin film channel area in OFETs with (a) silver electrodes and (b) gold electrodes. (c) (d) Polarized optical images in (a) and (b), respectively.

3.2 Characteristics of top contact OFETs

Figure 3.3 exhibits the transfer characteristics of the Ph-BTBT-10 thin film transistor in top contact configuration for two different S/D electrodes: silver and gold, respectively. The electrical characteristics extracted from Fig. 3.3 are summarized in Table 3.1. Ph-BTBT-10 thin films transistor using silver S/D electrodes exhibits mobility of 8.2 cm^2/Vs and on/off current ratio exceeds 10^7, which is similar to that of the OFET using gold S/D electrodes. On current of the Ph-BTBT-10 thin film transistor using silver S/D electrodes reached about 1 mA in lower gate voltage than that of OFET using gold S/D electrodes. In addition, Ph-BTBT-10 OFETs using silver S/D electrodes show ideal transfer characteristics, leading to the superior threshold voltage (V_{th}) and subthreshold swing (SS) to those of gold S/D electrodes.

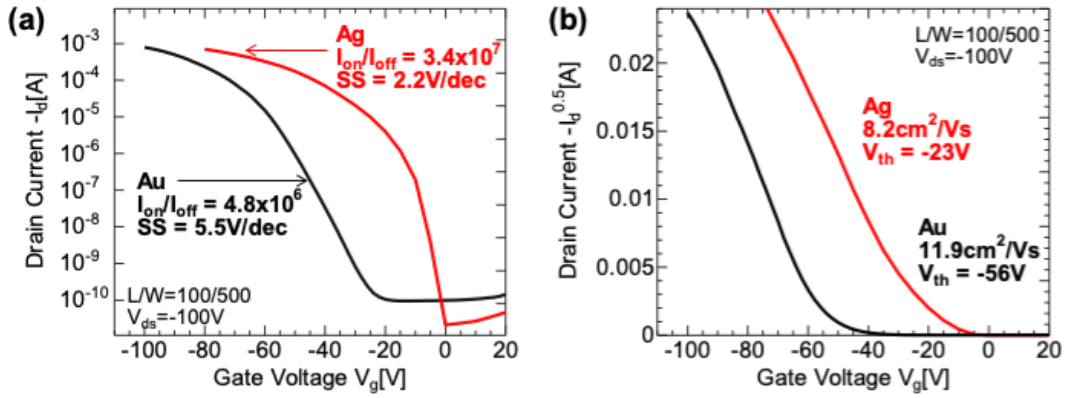

Figure 3.3 Transfer characteristics of top-contact Ph-BTBT-10 OFETs using silver (Red) and gold (Black) S/D electrodes, respectively. Y-axes are (a) logarithmic scale of drain current and (b) linear scale of square roof of drain current as a function of gate voltage.

Table 3.1 Electrical characteristics of top-contact Ph-BTBT-10 OFETs using silver (Ag) and gold (Au) S/D electrodes, respectively.

Electrodes	μ [cm^2/Vs]	I_{ON}/I_{OFF}	V_{th} [V]	SS [V/dec]
Ag	8.2	3.4×10^7	-23	2.2
Au	11.9	4.8×10^6	-56	5.5

Focusing on the threshold voltage, the threshold voltage of Ph-BTBT-10 OFET with silver and gold S/D electrodes presented -23 V and -56 V, respectively, showing a great improvement in Ph-BTBT-10 OFETs with silver S/D electrodes. Typically, the interface between the semiconductor and the gate insulator is considered a critical factor for determining threshold voltage and subthreshold swing. However, contact resistance, as well as the interface between the semiconductor and the gate insulator, can change the negative shift of threshold voltage for the p-channel transistors. High contact resistance leads to late channel accumulation. So, the drain current of OFETs with high contact resistance is decreased compared to that of OFETs with ohmic contact in a limited measurement time. Most of the OFETs present a decrease in contact resistance as gate voltage increases. The drain current greatly decreases at low gate voltage, while the drain current at the high voltage hardly decreases, consequently, the non-ideal transfer curve arises and the apparent threshold voltage is increased [7]–[9], as shown in Fig. 3.4. Also, the drain current is suppressed compared to the ideal drain current, especially in the subthreshold region, hence, the apparent subthreshold swing is increased.

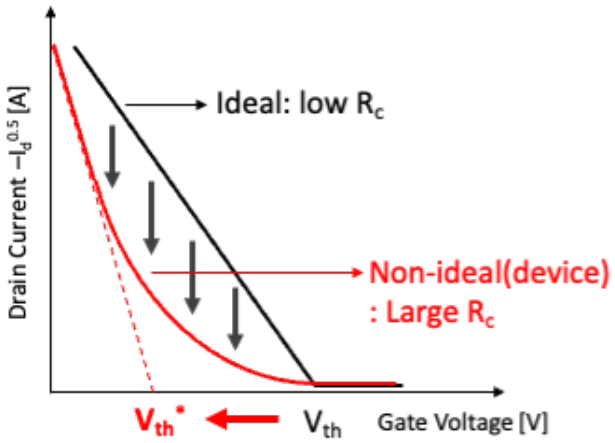

Figure 3.4 Conceptual illustration for transistor characteristics of OFETs with ideal and non-ideal

In this chapter, except for S/D electrode materials, all materials were prepared as the same ones, and all processes were conducted concurrently to reduce the variations of different conditions. So, it cannot be considered that the interface between the semiconductor and gate insulator affects dominantly for the performance of OFETs. Therefore, it can be concluded that the origin of the large reduction in the threshold voltage is attributed to the small contact resistance.

3.2.1 Contact resistance analyzed by transfer length method

In order to further analyze the contact resistance effect, the transfer length method (TLM) analysis was used. As mentioned in Chapter 2, the contact resistance was extracted by using the following equation:

$$R_{total} = R_{ch} + R_C$$

$$R_{total} \times W = \frac{L}{\mu C_i (V_g - V_{th})} + R_C \times W$$

Figure 3.5(a) shows the TLM result of Ph-BTBT-10 OFETs using Ag S/D electrodes. The transfer characteristics of OFETs with silver S/D electrodes in the linear region were obtained at source/drain voltage of -5 V in each channel length 20, 30, 50, 70, and 100 μm. The contact resistance can be extracted from a linear plot of R_{total}, by obtaining the intersection with the y-axis in Fig. 3.5(a), and contact resistance for top-contact configuration Ph-BTBT-10 OFETs using silver S/D electrodes at gate voltage of -80 V was extracted to be about 0.49 kΩcm. In addition, the contact resistance of Ph-BTBT-10 OFETs using silver S/D electrodes was compared to those of gold S/D electrodes. As for the OFETs using gold S/D electrodes, the previous research data was referenced and the transfer characteristics of OFETs with silver S/D electrodes in the linear region were obtained at source/drain voltage of -4 V [5]. The comparison results were plotted in Fig. 3.5(b) and the extracted contact resistance values at Vg of -80V were summarized in Table 3.2. It can be confirmed that the contact resistance of Ph-

BTBT-10 OFETs using silver S/D electrodes, 0.49 kΩcm, are smaller than those of gold S/D electrodes, 2.7 kΩcm. As shown in Fig. 3.5(b), the contact resistance strongly depends on gate voltage in Ph-BTBT-10 OFET with gold S/D electrodes, which increases apparent threshold voltage, as mentioned in the former section (Fig. 3.4).

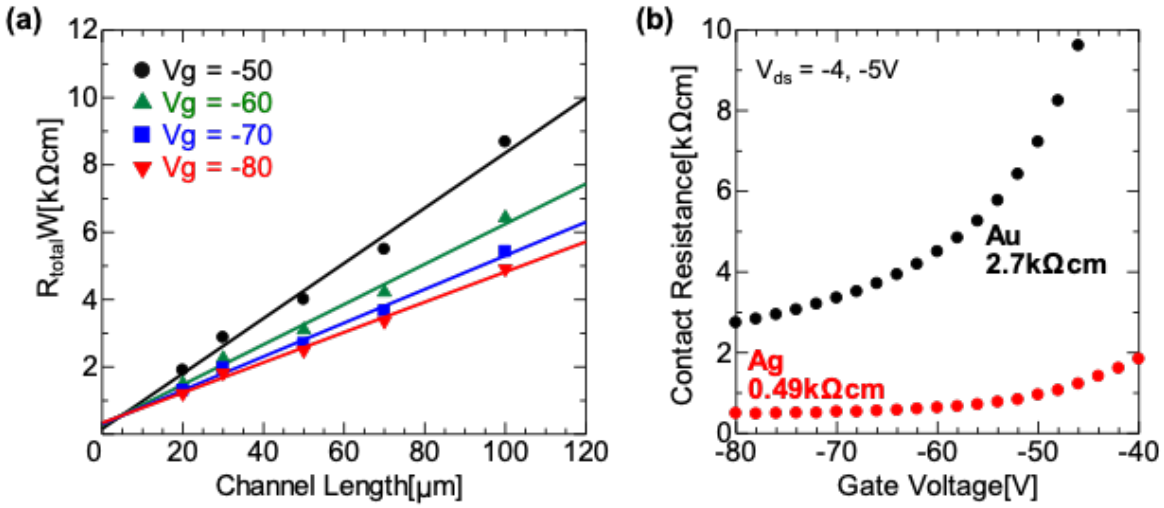

Figure 3.5 Transfer length method results for Ph-BTBT-10 OFETs using silver S/D electrodes. (a) Total resistance as a function of channel length. (b) Contact resistance of Ph-BTBT-10 OFETs with silver (Red) and gold (Black) S/D electrodes as a function of gate voltage.

Table 3.2 Summarized results for contact resistance Ph-BTBT-10 OFETs using silver (Ag) and gold (Au) S/D electrodes at gate voltage of -80V.

Electrodes	Ag	Au
R_cW [kΩcm]	0.49	2.7

3.2.2 Work functions of metals and HOMO level of Ph-BTBT-10

It has been reported that the performances of OFETs with silver S/D electrodes are generally inferior to those with gold S/D electrodes due to the low work function of silver. However, Ph-BTBT-10 OFETs using silver S/D electrodes did not match these results as shown in the former section. Therefore, firstly the energy level of electrode metals and Ph-BTBT-10 were investigated. The samples for evaluation of the work function of silver and gold and were

measured by photoemission spectroscopy in the air (PYSA: Riken Keiki AC-3). The highest occupied molecular orbital (HOMO) level of Ph-BTBT-10 is measured as -5.5 eV, as shown in Fig. 3.6(a). The work functions of silver and gold were 4.6 eV and 5.0 eV, respectively, as shown in Fig. 3.6(b). The hole injection barriers of Ph-BTBT-10 (HOMO level -5.5 eV) from silver and gold electrodes are estimated as 0.9eV and 0.5eV, respectively, as shown in Fig. 3.6(c). The result indicates the hole injection from gold electrodes is easier than that from silver electrodes, however, the contact resistance of Ph-BTBT-10 OFETs using silver S/D electrodes, 0.49 kΩcm, is smaller than that of gold S/D electrodes, 2.7 kΩcm, as shown in Table 3.2. For top-contact configuration OFET, contact resistance consists of injection resistance and access resistance. Injection resistance exists between S/D electrodes and Ph-BTBT-10 and access resistance exists between the contacting interface of S/D electrodes and the transport channel near the gate insulator. Carriers are not accumulated in this access resistance path, thus, access resistance is the main component of contact resistance in top-contact configuration [10]–[12].

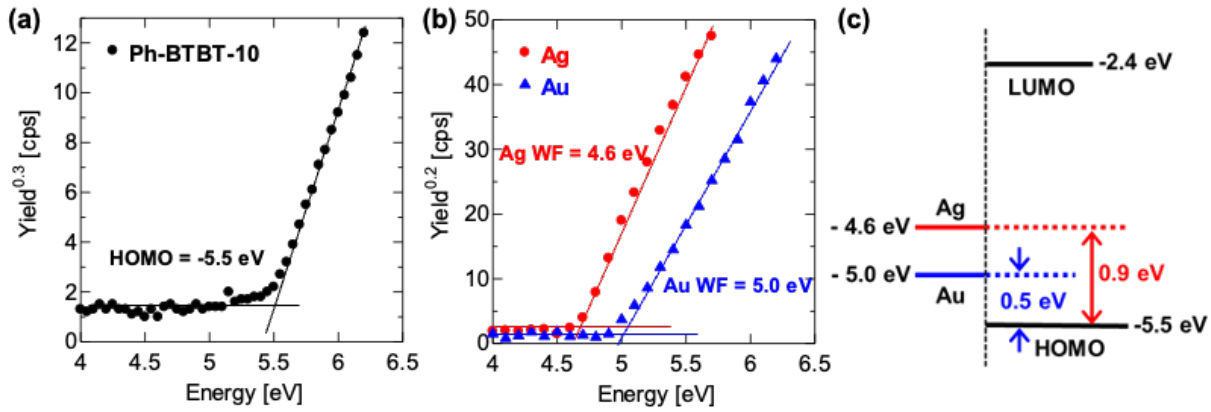

Figure 3.6 (a) The highest occupied molecular orbital (HOMO) of Ph-BTBT-10 (b) Work functions (WF) of silver and gold electrodes, respectively. (c) Energy diagram of the HOMO level of Ph-BTBT-10 and the work functions of silver and gold.

3.3 Effect of silver penetration

Generally, OFETs using silver S/D electrodes show poor properties because of its high hole injection barrier than those of gold S/D electrodes. However, Ph-BTBT-10 OFETs using silver S/D electrodes exhibited similar or better performance in top contact configuration. It is a very interesting result; therefore, some possible reasons can be discussed. It is assumed one possible reason is that silver metal clusters can be easily penetrated into Ph-BTBT-10 semiconductor layer upon deposition of the contact metal.

3.3.1 Observation by TOF-SIMS

To analyze the differences in penetration into Ph-BTBT-10 layer between Ag electrodes and Au electrodes, time-of-flight secondary ion mass spectrometry (TOF-SIMS) was investigated. TOF-SIMS is capable of elemental mapping with nanometer resolution [13], [14], so it enables us to observe the silver and gold distribution into the Ph-BTBT-10 layer. Figure 3.7 is the simplification of TOF-SIMS depth profiles for Ph-BTBT-10 layer with silver and gold (30 nm) electrodes layer, respectively. Each sample was prepared Ph-BTBT-10 spin-coated in thickness of about 30nm, and silver and gold electrodes were vacuum deposited in thickness of 30nm, respectively. In the case of the Ph-BTBT-10 layer with silver electrodes, sulfur ions originating from Ph-BTBT-10 were observed from the beginning as shown in Fig. 3.7(a). On the other hand, in the case of the Ph-BTBT-10 layer with gold electrodes, only gold ions appeared for the first 20 sec, and then sulfur ions emerged as shown in Fig. 3.7(b). These results can be considered as silver penetrated into the Ph-BTBT-10 layer deeply resulting in the Ph-BTBT-10 molecules appearing up to the surface of silver electrodes as shown in Fig. 3.7(c). Whereas gold hardly penetrates into the Ph-BTBT-10 layer because there is only gold layer for the first 20 sec, as shown in Fig. 3.7(d).

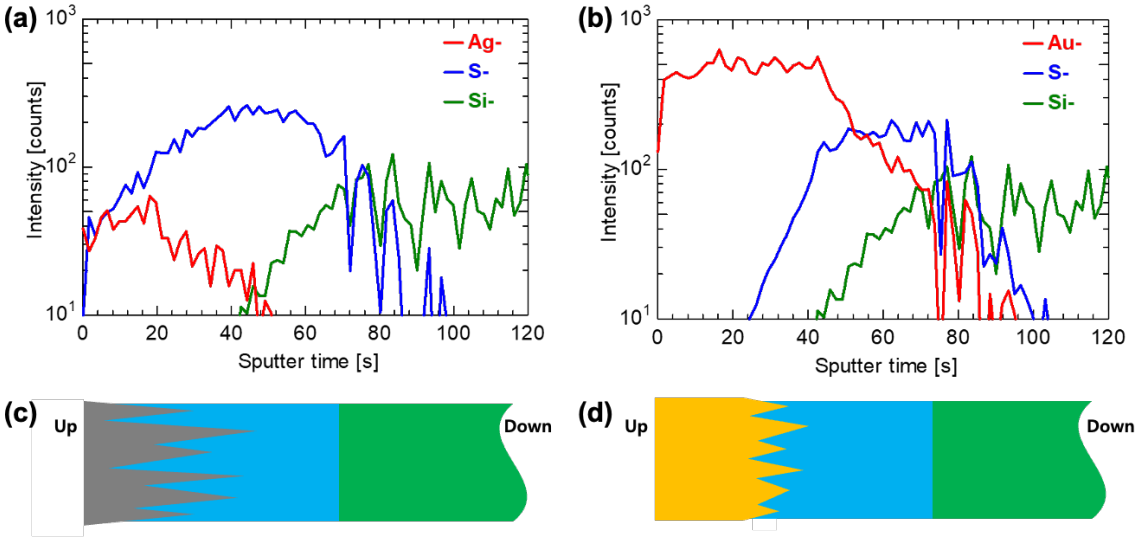

Figure 3.7 Depth profiles of metal/Ph-BTBT-10/substrate measured by TOF-SIMS. Metals are (a) silver (Ag) and (b) gold (Au), respectively. (c) (d) Schematic illustrations of the distribution of silver and gold based on the TOF-SIMS depth profiles in (a) and (b), respectively.

3.3.2 Observation by SEM

Cross-section profiles were observed by scanning electron microscope (SEM) to observe the interface between Ph-BTBT-10 layer and the metal electrodes layer. The samples were prepared for SEM analysis. Each electrode vacuum-deposited on a whole Ph-BTBT-10 layers, and the thickness of silver and gold electrodes were 100 nm and 30 nm, respectively. According to SEM analysis, the interface between Ph-BTBT-10 layer and the silver electrodes appeared very rough as shown in Fig. 5, in which the red dot line guided the interface between silver/Ph-BTBT-10/substrate. Whereas the interface between Ph-BTBT-10 layer and gold electrodes was flat as shown in the inset of Fig. 5 [15]. These results also showed that the penetration of silver and gold have differences, and it indicates the silver electrodes penetrated into Ph-BTBT-10 layer.

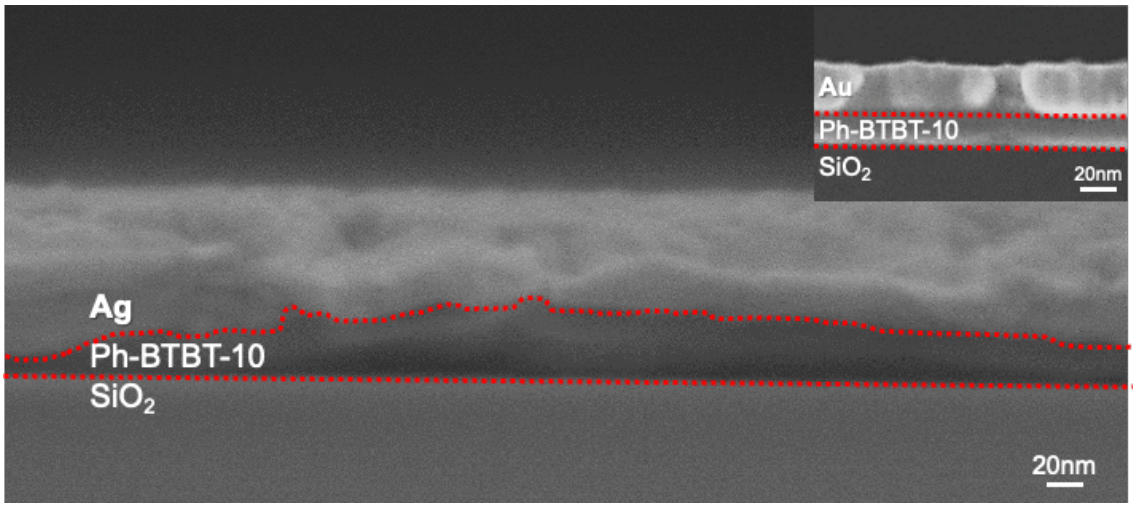

Figure 3.8 Cross-section images of silver/Ph-BTBT-10/substrate observed by SEM The inset shows cross-section image of gold/Ph-BTBT-10/substrate. The thickness of vacuum-deposited silver and gold electrodes were 100 nm and 30 nm, respectively.

3.3.3 Observation by XRR

X-ray reflectometry (XRR) is used to determine thickness, density, and roughness for single and multilayer stacks on semiconductor wafers. In the XRR measurement, two different samples were fabricated and compared. One is the silver electrodes were vacuum deposited on the Ph-BTBT-10 layer and then silver electrodes were etched to observe the surface roughness. The other is a pristine Ph-BTBT-10 layer without any treatment. The pattern-fitting process between the measured and the calculated XRR pattern preceded. In Fig. 3.9, red lines are measured data, blue lines are fitting of experimental data using GlobalFit software (provided by Rigaku corporation), and gray lines are residual. Also, each profile is multiplied by a factor of 10 for easy visualization. As shown in Fig. 3.9 and Table 3.3, the root mean square (RMS) of Ph-BTBT-10 with etched Ag surface roughness is bigger than that of pristine Ph-BTBT-10, 2.00 nm and 0.80 nm, respectively. Furthermore, the density of silver silver-etched Ph-BTBT-10 layer is lower than that of the pristine Ph-BTBT-10 layer. It is implied that some gaps might be created in Ph-BTBT-10 layer due to a disorder of molecular alignment derived from the penetration of silver into Ph-BTBT-10 layer.

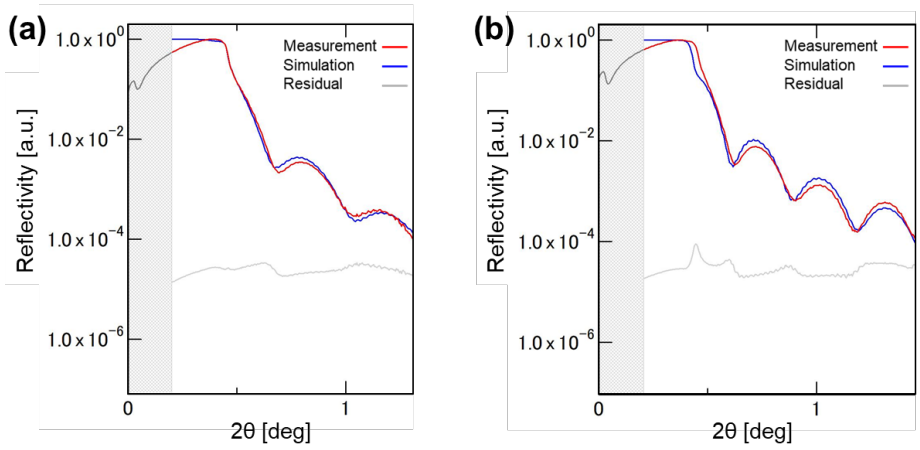

Figure 3.9 X-ray reflectivity profiles of Ph-BTBT-10 layer with (a) silver electrodes etched and (b) pristine, respectively. Red lines are measured data, blue lines are fitting of experimental data using GlobalFit software (provided by Rigaku corporation), and gray lines are residual. Each profile is multiplied by a factor of 10 for easy visualization.

Table 3.3 Fitting parameters of Fig. 3.9

	Ag etched			Pristine		
	Thickness [nm]	Roughness [nm]	Density [g/cm^3]	Thickness [nm]	Roughness [nm]	Density [g/cm^3]
Ph-BTBT-10	22.23	2.00	0.84	27.50	0.80	1.38
SiO_2	-	1.18	2.38	-	1.01	2.2

3.3.4 Result and discussion

Other organic semiconductors such as pentacene, TIPS-pentacene, and dibenzotetrathiafulvalene [1]–[4] showed higher OFETs performance with gold electrodes than those with silver electrodes. Table 3.4 is comparison of contact resistance between the Ph-BTBT-10 OFETs and pentacene OFETs [1], [16] as different S/D electrodes, silver and gold, respectively. Otherwise, in the case of 2,7-dioctyl[1]benzothieno[3,2-b][1]benzothiophene (C8-BTBT) OFETs performance with Ag S/D electrodes showed similar to those of gold S/D electrodes [17]. Therefore, it is assumed that the alkyl chain and exhibition of the liquid crystal phase help to make disorder of molecular alignment, which enhances silver penetration. The

results imply that silver electrodes were penetrated into Ph-BTBT-10 layer more deeply compared to those with gold electrodes, decreasing access resistance, which is the dominant element of the contact resistance in top contact configuration. Furthermore, SEM and XRR results indicated that the interface area between Ph-BTBT-10 layer and silver electrodes is larger than that between Ph-BTBT-10 layer and gold electrodes, hence, this larger interface area ensures the increase of the carrier injection area and results in achieving the small injection resistance of Ph-BTBT-10 OFET with Ag S/D electrodes. Moreover, as silver penetrated into Ph-BTBT-10, molecular orientation and ordering at the interface between metal and Ph-BTBT-10 are disturbed and crystallinity is decreased, so the distribution of HOMO level of Ph-BTBT-10 is broadened as shown in Fig. 3.10. As a result, injection sites are increased, and this phenomenon can also reduce injection resistance. Therefore, it can conclude that Ph-BTBT-10 OFETs with silver S/D electrodes showed comparable and superior performance compared to those with gold. Moreover, in general, silver interacts very well with sulfur, thus, there might be an interaction between Ag electrodes and the sulfur atom of BTBT core which promotes Ag penetration.

Table 3.4 Summarized results for contact resistance as different organic semiconductors and electrode metals.

Contact Resistance	Electrodes metal (evaporated)	
[Ωcm]	Ag	Au
Ph-BTBT-10	0.49k	2k
Pentacene	60k	8k

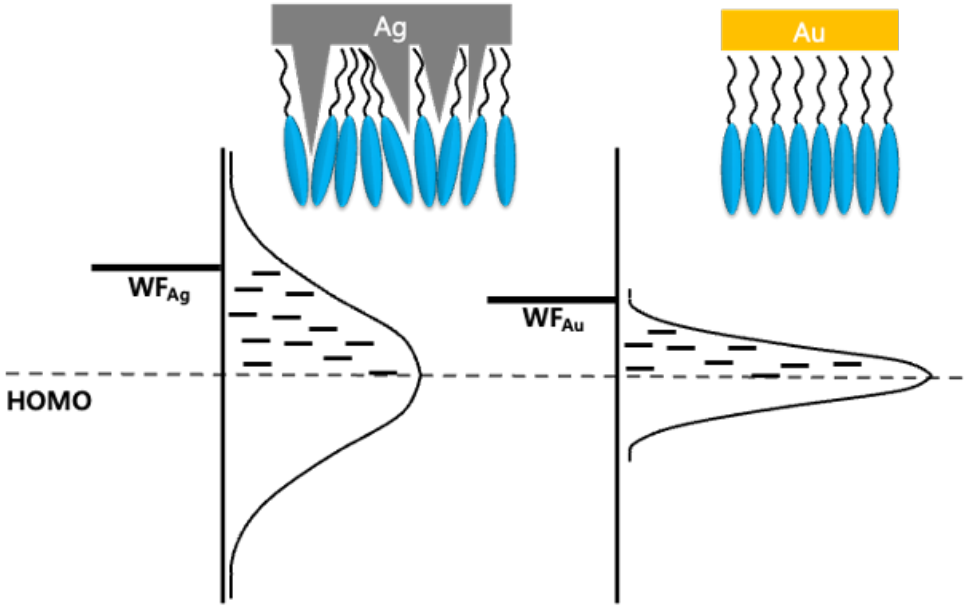

Figure 3.10 Schematic illustration of cross-section of polycrystalline Ph-BTBT-10 film and metals on Ph-BTBT-10 films.

3.4 Difference of the crystal structures of Ph-BTBT-10

Ph-BTBT-10 has two crystal structures, i.e., monolayer and bilayer crystal structures. Monolayer crystal structure is similar to the structure of liquid crystal phase and the alkyl chain parts have disordered structure. On the other hand, bilayer crystal structure is similar to the structure of most stable crystals fabricated from solution and the alkyl chain part have highly order. For gold electrode on the polycrystalline thin films of Ph-BTBT-10, the difference of contact surface due to these crystal structure can affect metal penetration into the Ph-BTBT-10 thin films [15]. So, the difference of crystal structure of Ph-BTBT-10 with silver S/D electrodes was investigated. The experiment was carried out in two different fabrication processes at the same time to reduce the variations caused by a different crystalline condition such as Ph-BTBT-10 polycrystalline thin films having monolayer crystal structure and bilayer crystal structure. Table 3.4 shows the flow chart of the fabrication processes each other. In the chart, thermal annealed (TA) before deposition of electrodes means that the OFET devices were thermal annealed before vapor deposition of the metal electrode. In other words, electrodes were formed on the bilayered polycrystalline Ph-BTBT-10 thin films. On the other hands, thermal annealing after deposition of electrodes indicates that metal electrodes were formed first on the monolayered polycrystalline Ph-BTBT-10 thin films, and then thermal annealing after the metal electrodes deposited by vacuum evaporation. The experiment of the same condition was tested several times in order to confirm reproductivity.

As shown in Fig. 3.11, for the monolayer crystal structure, gold metal can penetrate into Ph-BTBT-10 layer densely and deeply. Therefore, the contact between electrodes and Ph-BTBT-10 thin films improved. In the case of gold electrodes, by vapor deposition of electrodes on monolayer crystal structure thin film, and then thermally annealing, the contact resistance lowered 2 kΩcm to 0.8 kΩcm as shown in Table 3.5.

Table 3.4 Flow chart of the fabrication processes

TA before deposition of electrodes : on bi-layered polycrystalline films	TA after deposition of electrodes : on monolayered polycrystalline films
Substrate cleaning	
Fabrication of Ph-BTBT-10 thin-film by spin coating	
Thermal annealing (120℃, 15min)	
deposition of metal electrodes by thermal evaporation (30nm)	
	Thermal annealing (120℃, 15min)

The devices deposited silver electrodes on bilayer crystal structure thin films of Ph-BTBT-10 after TA exhibited high current and carrier mobility and it is similar to the result of deposited gold on bilayer crystal thin films of Ph-BTBT-10 with. It may be ascribed to reason that it is more difficult to transform monolayer to bilayer crystal structures, especially at the surface when TA after the vapor deposition of metal electrodes. However, when it comes to TLM result, devices with silver electrodes exhibited no significant changes, regardless of the difference crystal structures as shown in Fig. 3.11, it showed contact resistance of average 0.4 kΩcm as shown in Fig. 3.12 and Table 3.5. It may imply that silver electrodes penetrate more easily into the semiconductor layer compared to gold electrodes and form contact deeply and densely. It's because there was no difference by the effect of the wide contact area formed by monolayer structure.

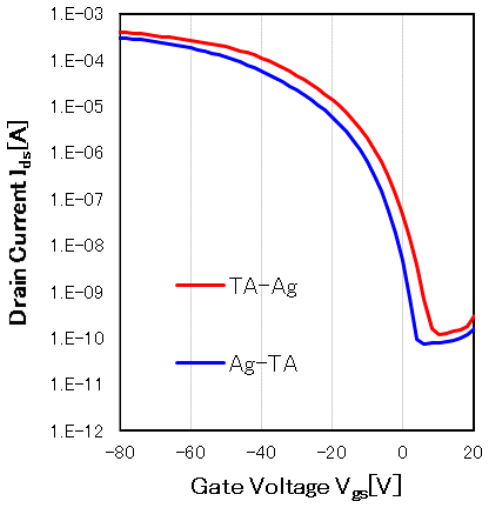

Figure 3.11 Transfer characteristics for OFETs with silver electrodes as different thermal annealing condition: thermal annealed before deposition of silver electrodes (TA-Ag) and after deposition of silver electrodes (Ag-TA)

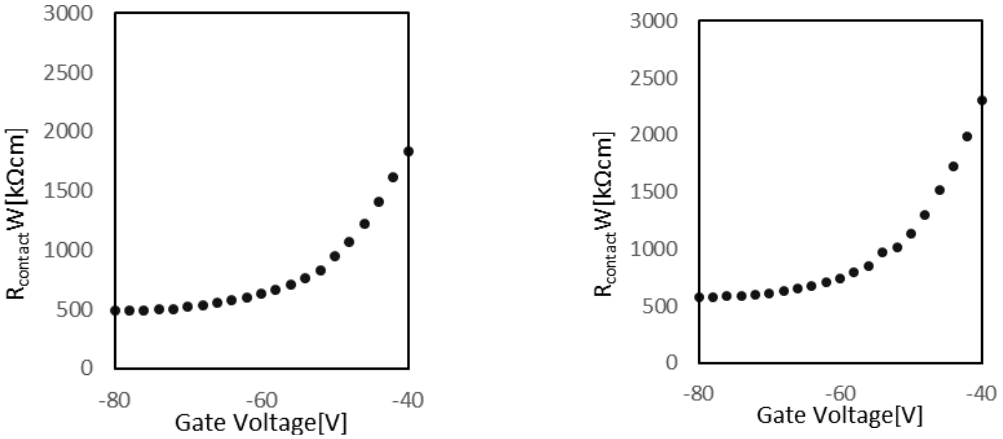

Figure 3.12 TLM results: contact resistance of OFETs with top contact silver S/D electrodes as different structure of Ph-BTBT-10 polycrystalline thin film. (a) TA before deposition of Ag electrodes (b) TA after deposition of Ag electrodes

Table 3.5 Summarized the results for contact resistance as different structure of Ph-BTBT-10 polycrystalline thin film: silver electrodes (Ag), gold electrodes (Au)

		Film structure	
		Monolayer	Bilayer
Contact resistance $R_C\ W[\Omega cm]$	Silver electrodes	0.4k	0.4k
	Gold electrodes	0.8k	2k

3.5. Conclusion

It has been demonstrated that the high-performance Ph-BTBT-10 OFETs with bottom-gate top-contact configuration with silver S/D electrodes exhibited high mobility of 8.2 cm^2/Vs and smaller threshold voltage than those with gold S/D electrodes. The contact resistance of Ph-BTBT-10 OFET with silver S/D electrodes is obtained as 0.49 kΩcm by TLM, which is less than those with gold S/D electrodes, 2.7 kΩcm. It was considered that the good performance of OFET with silver S/D electrodes did not come from the work function of silver electrodes, the silver metals are easily penetrated into Ph-BTBT-10 layer, decreasing the access resistance which is dominant for contact resistance. According to the cross-section analysis with SEM, silver electrodes appeared to be penetrated into Ph-BTBT-10 layer deeply with a rough interface between electrodes and Ph-BTBT-10 layer, while gold electrodes showed a relatively flattened interface. In addition, based on the depth profiles by TOF-SIMS, it can be inferred that the layer that exists only silver electrodes might be very thin, and the mixed layer of silver electrodes and Ph-BTBT-10 could be formed relatively up to the upper position, because the sulfur ion which indicated the existence of Ph-BBT-10 layer was observed at less than 5 s for silver electrodes, while gold electrodes appeared at over 20 s. In conclusion, silver electrodes were penetrated into Ph-BTBT-10 layer more deeply, decreasing access resistance [8-10], which is one of the elements of contact resistance. Therefore, it can be concluded that Ph-BTBT-10 OFET using silver electrodes in bottom-gate and top-contact configurations exhibited excellent electrical properties, thus, it implies that silver electrode is a promising candidate for high-performance and low-cost OFETs.

References

[1] M. Nakao, T. Manaka, M. Weis, E. Lim, and M. Iwamoto, “Probing carrier injection into pentacene field effect transistor by time-resolved microscopic optical second harmonic generation measurement,” *J. Appl. Phys.*, vol. 106, no. 1, p. 014511, 2009.

[2] S. Chung, J. Jeong, D. Kim, Y. Park, C. Lee, and Y. Hong, “Contact resistance of inkjet-printed silver source-drain electrodes in bottom-contact OTFTs,” *J. Disp. Technol.*, vol. 8, no. 1, p. 48, 2011.

[3] K. Shibata, K. Ishikawa, H. Takezoe, H. Wada, and T. Mori, “Contact resistance of dibenzotetrathiafulvalene-based organic transistors with metal and organic electrodes,” *Appl. Phys. Lett.*, vol. 92, no. 2, p. 023305, 2008.

[4] J. H. Kwon *et al.*, “Channel width effect for organic thin film transistors using TIPS-pentacene employed as a dopant of poly-triarylamine,” *Org. Electron.*, vol. 10, no. 4, p. 729, 2009.

[5] H. Iino, T. Usui, and J. I. Hanna, “Liquid crystals for organic thin-film transistors,” *Nat. Commun.*, vol. 6, p. 6828, Apr. 2015.

[6] H. Iino and J. I. Hanna, “Availability of liquid crystallinity in solution processing for polycrystalline thin films,” *Adv. Mater.*, vol. 23, no. 15, p. 1748, Apr. 2011.

[7] E. G. Bittle, J. I. Basham, T. N. Jackson, O. D. Jurchescu, and D. J. Gundlach, “Mobility overestimation due to gated contacts in organic field-effect transistors,” *Nat. Commun.*, vol. 7, p. 10908, Mar. 2016.

[8] Y. Xu *et al.*, “Precise Extraction of Charge Carrier Mobility for Organic Transistors,” *Adv. Funct. Mater.*, vol. 30, no. 20, p. 1904508, May 2020.

[9] T. Uemura *et al.*, “On the Extraction of Charge Carrier Mobility in High-Mobility Organic Transistors,” *Adv. Mater.*, vol. 28, no. 1, p. 151, Jan. 2016.

[10] B. Kumar, B. K. Kaushik, and Y. S. Negi, “Modeling of top and bottom contact structure organic field effect transistors,” *J. Vac. Sci. Technol. B*, vol. 31, no. 1, p. 012401, Jan. 2013.

[11] B. Chen, F. Aikawa, and E. Itoh, “Improvement of device performance of Ph-BTBT-10 field-effect transistors fabricated on a HfO2/alicyclic polyimide double-layered gate insulator,” *Jpn J Appl Phys*, vol. 61, no. SB, Feb. 2022.

[12] Q. Wang *et al.*, “Role of Schottky Barrier and Access Resistance in Organic Field-Effect Transistors,” *J. Phys. Chem. Lett.*, vol. 11, no. 4, p. 1466, Feb. 2020.

[13] C. W. T. Bulle-Lieuwma, W. J. H. Van Gennip, J. K. J. Van Duren, P. Jonkheijm, R. A. J. Janssen, and J. W. Niemantsverdriet, “Characterization of polymer solar cells by TOF-SIMS depth profiling,” *Appl. Surf. Sci.*, vol. 203, p. 547, Jan. 2003.

[14] T. Zhang *et al.*, “Profiling the organic cation-dependent degradation of organolead halide perovskite solar cells,” *J. Mater. Chem. A*, vol. 5, no. 3, p. 1103, 2017.

[15] K. Aburada, “Master thesis,” Tokyo Institute of Technology, 2020.

[16] S. Chung, J. Jeong, D. Kim, Y. Park, C. Lee, and Y. Hong, “Contact resistance of inkjet-printed silver source-drain electrodes in bottom-contact OTFTs,” *J. Disp. Technol.*, vol. 8, no. 1, p. 48, 2012.

[17] A. Ablat, A. Kyndiah, G. Houin, T. Y. Alic, L. Hirsch, and M. Abbas, “Role of Oxide/Metal Bilayer Electrodes in Solution Processed Organic Field Effect Transistors,” *Sci. Rep.*, vol. 9, no. 1, p. 6685, Dec. 2019.

Chapter 4
Sutdy on the bottom contact OFETs using silver source/drain elecotrodes

4.1 Introduction

In this chapter, the bottom-contact configuration OFETs with silver S/D electrodes are discussed. The top-contact configuration Ph-BTBT-10 OFETs with silver S/D electrodes showed comparable or superior performance to those with gold S/D electrodes. However, the top-contact structure OFETs generally have obstacles to the manufacturability application, that is, incompatibility with fabricating electrodes such as photolithographic processes, which can have small channel lengths, and solution processes, which can damage the organic layer at the deposition of silver ink and baking for metallization. Therefore, the bottom-contact configuration is a feasible geometry in practical applications. Unfortunately, the bottom contact OFETs suffer from lower performance because the bottom contact structures have poor contact performance between S/D electrodes and the semiconductor layers leading to high contact resistance. Therefore, interface engineering between electrodes and organic semiconductors is necessary to ensure an efficient charge carrier injection [1]–[3]. To form an ohmic contact, self-assembled monolayers (SAMs) treatments are investigated to improve the surface contact performance between the organic semiconductor and silver S/D electrodes.

4.1.1 Fabrication process of bottom contact OFETs

Ph-BTBT-10 OFETs investigated in this chapter are the bottom-gate bottom-contact type as shown in Fig. 4.1. As the bottom gate and a dielectric layer, Si/SiO_2 (300nm) were prepared and rinsed with an ultrasonic cleaner. Silver S/D electrodes were vacuum deposited using either a thermal evaporator or an electron-beam (E-beam) evaporator with metal shadow masks on substrates. The thickness of silver S/D electrodes was given a variety and experimented in order to inject an effective carrier, and it is demonstrated in the latter section. After the fabrication of silver S/D electrodes, self-assembled monolayer (SAMs) treatment was conducted immediately to keep silver electrodes from contaminating. SAMs treatment procedures were considered of two types, the immersing process and the vapor process. The detailed procedure, and the comparison will be explained in the latter section. Polycrystalline thin films of Ph-BTBT-10 were fabricated by spin coating at liquid crystal phase of 110 ℃ at 3000 rpm for the 30 s. After spin-coating Ph-BTBT-10 thin film, OFETs substrates were thermally annealed at 120 ℃ for 15 minutes. In addition, OFETs with gold S/D electrodes were fabricated following the same fabrication process and conditions to compare the performances of OFETs.

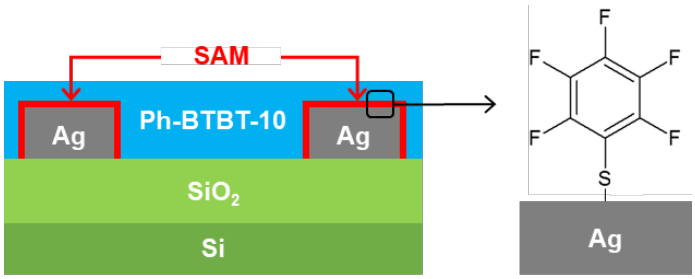

Figure. 4.1 Cross-sectional schematic of the bottom-gate bottom-contact OFET with SAM-treated silver S/D electrodes.

4.1.2 Challenge of silver electrodes

Figure 4.2 shows the output characteristics of Ph-BTBT-10 OFETs with silver and gold S/D electrodes, respectively, at the gate voltage of -60 V. In contrast to the top-contact OFETs with silver S/D electrodes which exhibited superior performance to those with gold S/D electrodes, the bottom-contact OFETs with silver S/D electrodes presented a significant difference showing inferior performance to those with gold S/D electrodes. For the OFETs with silver S/D electrodes, the current was severely reduced compared to those with gold S/D electrodes. In addition, an S-shaped curve in low drain voltage typifying the presence of large contact resistance is directly observed in the output curve of the silver S/D electrode device. It is attributed that generally OFETs with silver S/D electrodes have a bigger energy mismatch between the work function of the electrode and the HOMO level of Ph-BTBT-10 than those with gold electrodes as shown in Fig. 4.2 (b). This energetic misalignment can cause a high hole-injection barrier corresponding to high contact resistance. Therefore, to form an ohmic contact, the matching of the energy levels is essential for ensuring an efficient charge carrier injection [1]–[3].

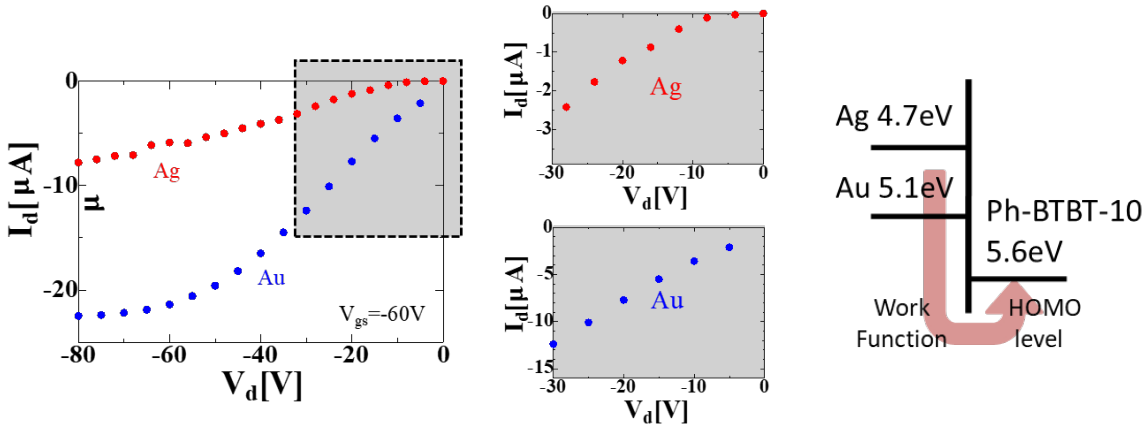

Figure 4.2 Output characteristics as different S/D electrodes metal: silver (red dot) and gold (blue dot) S/D electrodes, respectively.

4.2 Silver electrodes modified by self-assembled monolayer

It has widely been reported that the work function of metal electrodes can be tuned by using various dipolar self-assembled monolayers (SAMs) on the metal electrodes. SAMs are to play with the energy shift at the metal-semiconductor interface by deliberately introducing an interface dipole. The direction of the dipole moment controls that of the energy shift [4]–[7]. In this section, pentafluorobenzenethiol (PFBT) which is well-known as a modifier of both gold and silver electrodes was investigated [3]–[5], [8]–[11]. It is because Ph-BTBT-10 OFETs with gold S/D electrodes have been optimized on the PFBT treatment conditions. Therefore, first, OFETs with silver S/D electrodes were fabricated under the same condition which carried out for gold electrodes to optimize the condition of OFETs with gold electrodes. Except for electrodes materials, all fabrication process such as substrate cleaning, fabrication of thin film, and SAMs treatment were carried out simultaneously to apply for the same condition. Figure 4.4 (a) and (b) showed optical microscope images of the device with silver and gold, respectively, and it may be considered that properties of Ph-BTBT-10 thin-film had no significant difference.

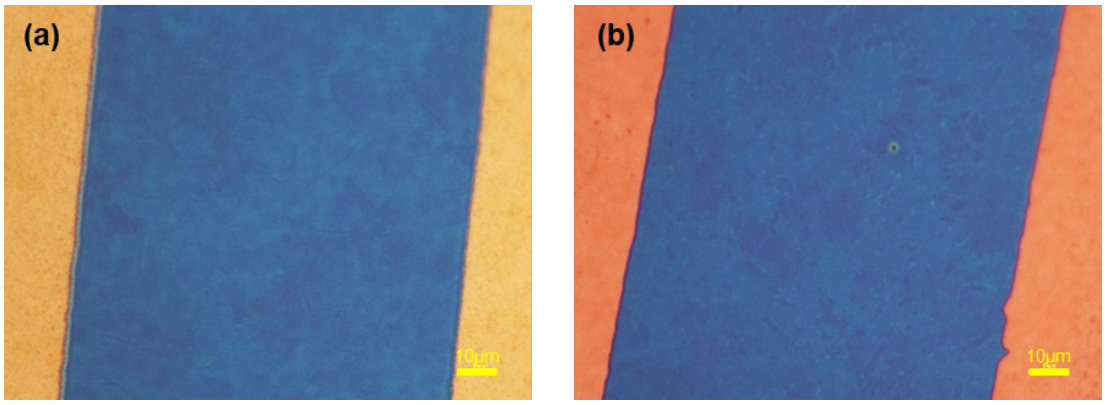

Figure 4.3 Optical microscope images of Ph-BTBT-10 thin film channel area in OFETs with (a) PFBT modified silver S/D electrodes and (b) PFBT modified gold S/D electrodes.

Figure 4.5 shows the results of the OFET performance with PFBT-treated gold and silver electrodes. For the device with gold electrodes, the average mobility of 3.72 cm^2/Vs and the highest mobility exceeding 6 cm^2/Vs were obtained. However, in the case of the silver electrode devices, on-current and mobility were lower than several orders of magnitude of those of gold, and the output curve showed still S-shape behavior related to the large contact resistance. Some devices exhibited lower on-current and mobility than those of its bare device even though the silver electrodes were modified with PFBT. Therefore, it is required to confirm and to explore what condition is optimal to make high performed OFETs with Ag devices.

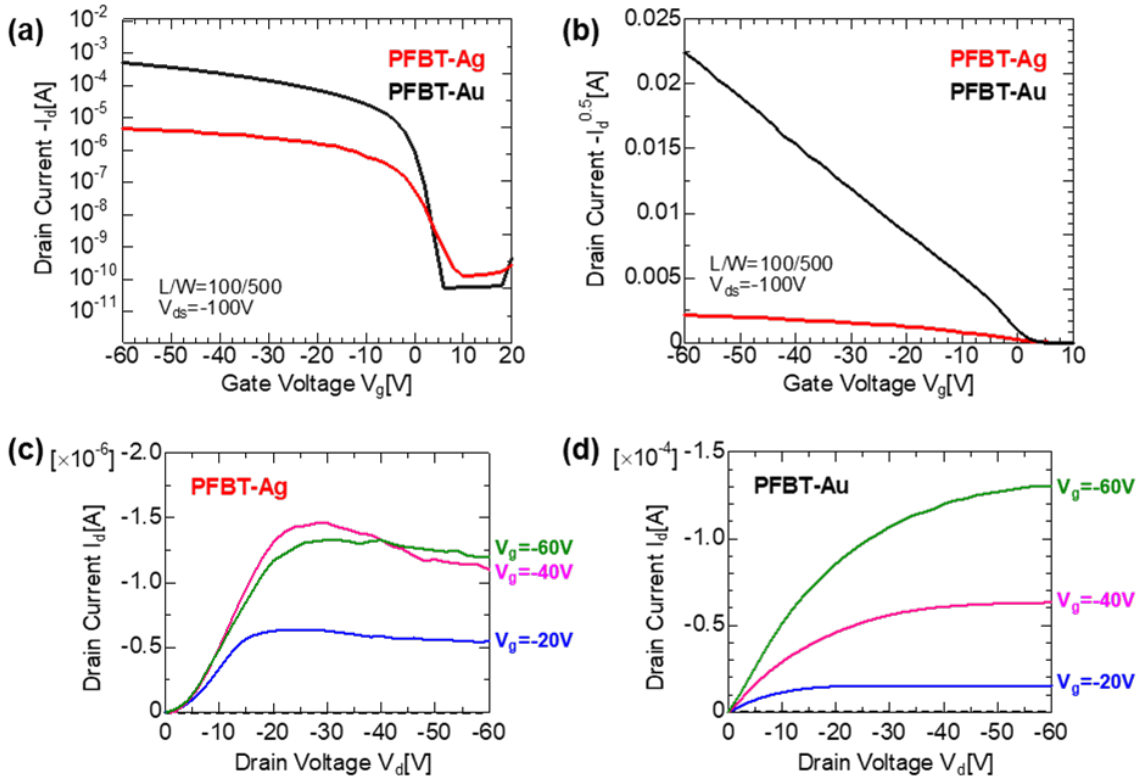

Figure 4.4 Transfer characteristics of bottom-contact Ph-BTBT-10 OFETs with silver (red) and gold (black) S/D electrodes, respectively. Y-axes are (a) logarithmic scale of drain current and (b) linear scale of square roof of drain current as a function of gate voltage. Output characteristics of bottom-contact Ph-BTBT-10 OFETs PFBT-treated (c) silver and (d) gold S/D electrodes, respectively.

Table 4.1 Electrical characteristics of the Ph-BTBT-10 OFETs as different S/D electrodes materials, silver (Ag) and gold (Au) respectively.

	PFBT modified Ag	PFBT modified Au
Mobility [cm^2/Vs]	0.14	3.72
On current [A]	3.8×10^{-6}	3.8×10^{-4}

4.2.1 Contact angles

PFBT was widely used as a modifier of silver S/D electrodes exhibiting improved OFET performance [4], [9]–[11]. However, while the result which was conducted under the same experiment condition OFETs with gold S/D electrodes showed improved OFET performances, OFETs with silver S/D electrodes did not show a significant difference compared to those with pristine silver S/D electrodes. Therefore, to confirm the existence of a PFBT layer on silver S/D electrodes, the water contact angles were measured. The contact angle of metal surfaces is important for the morphology of the resulting film onto the S/D electrode. This is because the PFBT-modified surface has hydrophobic properties and exhibits higher contact angles in terms of the differences in the wettability on the surface. The surface modifications were treated in the glove box and contact angle measurements were performed in air at room temperature. As shown in Fig. 4.6, the contact angle of the water drops was different depending on whether or without SAM treatment. The clean, bare silver electrodes without SAM modification with PFBT typically had contact angles between 65° and 72° as shown in Fig. 4.6 (a). Furthermore, the contact angles of the PFBT-modified silver electrode surfaces measured between 95° and 105°, as shown in Fig. 4.6(b). As a result, silver electrodes in this experiment were modified by PFBT practically, hence, it is required to investigate other parameters that

affect charge injection.

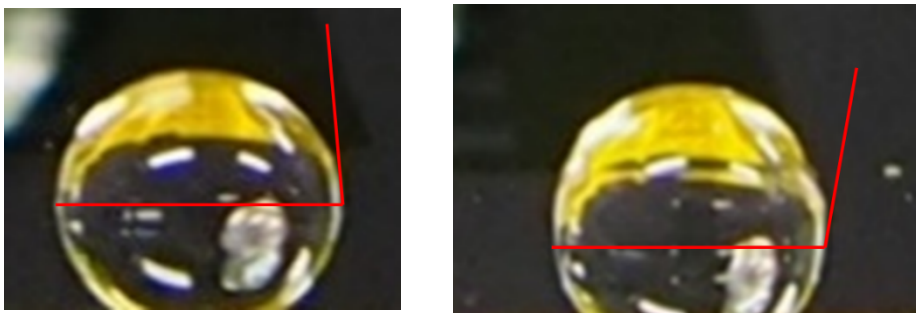

(a) Bare Ag θ=85.87°　　(b) PFBT 100mmol/L θ=99.91°

Figure 4.5 Images of contact angle measurement for (a) untreated silver S/D electrodes and (b) PFBT-treated silver S/D electrodes.

4.2.2 Thickness of silver electrodes

In the case of the bottom contact structure, charge carrier injection is performed from both the top and the side of S/D electrodes, therefore, the thickness of the S/D electrode is one of the factors that affect the carrier injection. According to Jung et al., for gold S/D electrode, when the thickness of electrodes is less than 30nm pentacene OFETs exhibited significantly worse performance compared to those with thicker than 30nm [12]. Thereby, it is necessary to control the thickness of silver S/D electrodes, since charge carrier injection from the side of electrodes greatly affects when the thickness of electrodes thinner. In the former section, Ph-BTBT-10 OFETs with silver S/D electrodes which is the thickness of 30 nm presented poor performance unlike those with gold S/D electrodes. Especially, the result showed unstable which cannot be achieved reproductivity. A couple of the previous research studies using either vapor deposited silver S/D electrodes or other methods was referenced, and most of the research work used the thickness of the silver electrode from 50 nm to 70 nm [10], [13], [14]. Therefore, in order to confirm whether or not the thickness of the 30 nm silver electrode fabricated so far is in a range that is greatly

affected by the side, 50 nm and 70 nm thickness of silver electrode devices were manufactured. Each device was evaluated the characteristics compared to the 30 nm thickness of silver S/D electrode device.

Figure 4.7 shows the transfer and output characteristics as the various thickness of silver S/D electrodes, 30 nm, 50 nm, and 70 nm, respectively. Table 4.2 summarized the mobility and threshold voltage extracted from Fig. 4.7. All OFET devices were fabricated with PFBT modified silver S/D electrodes. OFETs with 70 nm thickness of electrodes exhibited remarkably improved performance that exceeding 1 cm^2/Vs of mobility while 30 nm and 50 nm showed poor properties. In addition to mobility, it showed improved S-shape behavior in the small drain voltage as shown in the output curve. The result suggests that OFETs with silver electrodes require thicker electrodes than gold electrodes to achieve optimization condition. Therefore, it can be concluded that the thickness electrodes are correlated to improve the charge carrier injection, and required to optimize the thickness, that is 70 nm for the silver electrodes.

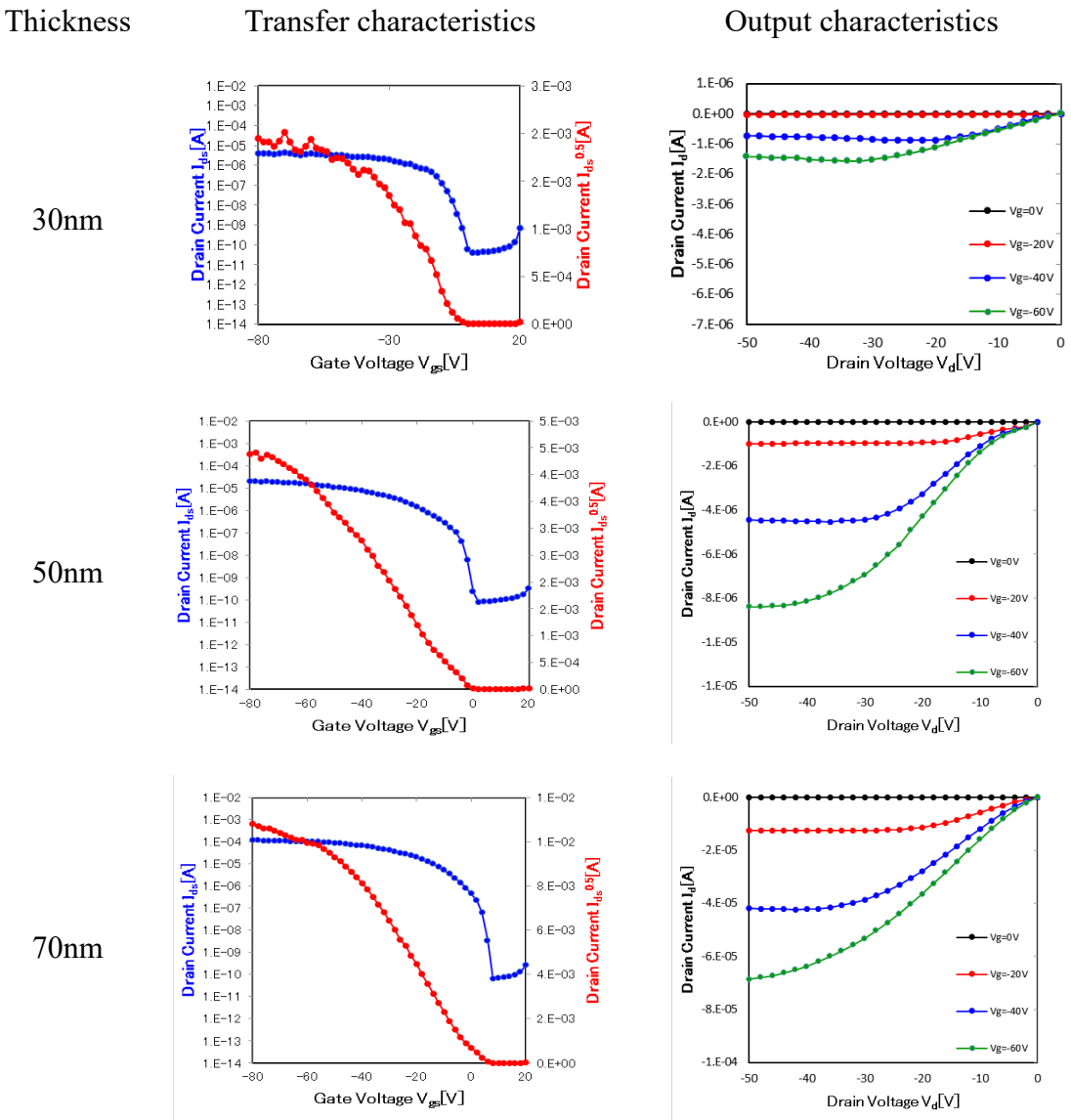

Figure 4.6 Transfer and output characteristics as the various thickness of silver S/D electrodes: (a)(b) 30 nm, (c)(d) 50 nm, and (e)(f) 70 nm, respectively.

Table 4.2 Electrical characteristics of the Ph-BTBT-10 OFETs as the various thickness of silver (Ag) S/D electrodes: 30 nm, 50 nm, and 70 nm respectively.

Thickness of Ag	30 nm	50 nm	70 nm
Mobility [cm^2/Vs]	0.14	0.26	1.7
V_{th} [V]	-2.5	-10.2	0.3

4.2.3. Solution concentrations of SAM treatment

In order to confirm the effect of solution concentration of SAM treatment, contact angle and OFET performance were investigated for devices with high (100 mmol/L) and low (5 mmol/L) solution concentrations of SAM treatment. Two samples were prepared under each SAM treatment condition in the glove box and contact angles were measured in the air. Ultrapure water was dropped on each substrate at three locations. While untreated silver electrodes had a contact angle of 78 °, both SAM-treated silver electrodes showed an increase in contact angles of about 95 °. Therefore, it is clear that the low-concentration (5 mmol/L) PFBT solution also formed the adhesion of SAM to the electrode surface and the modification of the electrode surface condition. Regarding different PFBT concentrations, the high-concentration PFBT solution (100 mmol/L) showed a slightly higher contact angle than that of the low-concentration PFBT solution, as shown in Fig. 4.7(b) and (c). But the high-concentration PFBT solution (100 mmol/L) presented a larger deviation, as shown in Fig. 4.7(d). Therefore, the OFET performance was compared so as to increase the reliability of the results.

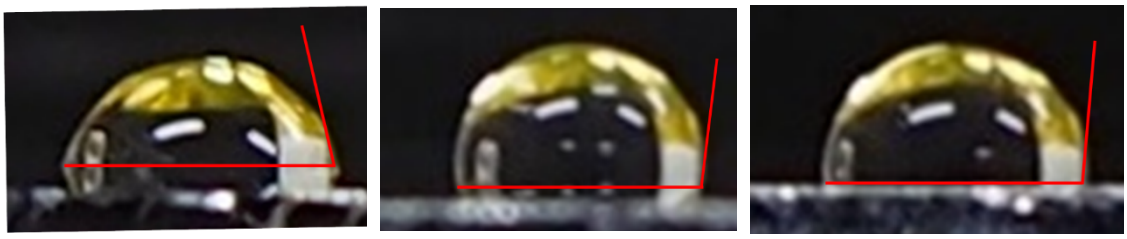

(a) Bare Ag θ=77.51° (b) PFBT 100mmol/L (c) PFBT 5mmol/L θ=95.00°

Figure 4.7 Contact angle as different conditions of PFBT treatment. Images of (a) bare silver, silver treated by (b) high PFBT solution (100 mmol/L), (c) low PFBT solution (5mmol/L).

Figure 4.8 shows the transfer characteristics of Ph-BTBT-10 FET with silver S/D electrodes modified under the different conditions of PFBT treatment. From the linear region of the transfer characteristics as shown in Fig. 4.8, it can be seen that the characteristics are improved depending on the presence of the PFBT treatment. The mobility of OFETs as different concentrations of PFBT were 1.36 cm^2/Vs at 100 mmol/L and 1.34 cm^2/Vs and at 5 mmol/L, respectively. As expected in contact angles, there is no significant difference as the concentration of PFBT solution. Therefore, it is considered that the condition of 5 mmol/L is enough concentration to cover the surface of silver electrodes and can realize a low-cost process.

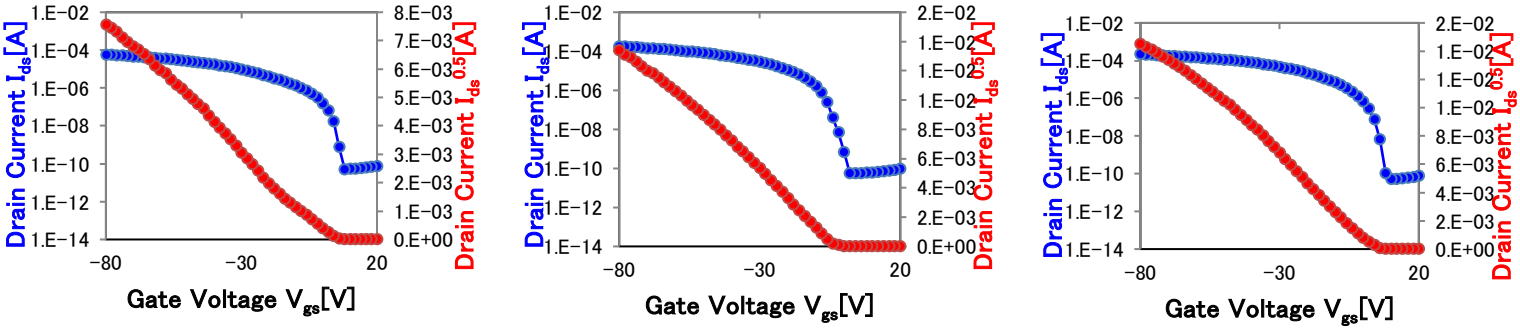

(a)Bare
μ=0.43cm^2/Vs, Vth=-2.30V

(b) PFBT 100mM 20min
μ=1.47cm^2/Vs, Vth=-4.00V

(c) PFBT 5mM 2min
μ=1.67cm^2/Vs, Vth=1.19V

Figure 4.8 Transfer characteristics of Ph-BTBT-10 FET with (a) pristine, (b) high concentration (100 mmol/L) PFBT-treated, and (c) low concentration PFBT-treated 5 mmol/L silver S/D electrodes.

Table 4.3 OFETs mobility as different conditions of PFBT treatment

PFBT condition	Bare	100 mmol/L 20min	5 mmol/L 2min
Mobility[cm^2/Vs]	0.31±0.07	1.36±0.20	1.34±0.41
Number of units	2	4	4

4.2.4. Vapor process of SAM treatment

In order to reduce the process steps and time, SAMs treatment was conducted by ambient-pressure vapor deposition. Silver S/D electrodes-patterned substrates were placed on the hot plate heated at 100 ℃ and exposed to SAM materials vapor for 15 minutes by capping with a petri dish. In order to confirm the SAMs modification for silver electrodes, contact angles were measured. The contact angle of pristine silver electrodes was 81°, and after modifying silver electrodes with PFBT SAMs, the contact angles of silver were changed to 102 ° as shown in Fig. 4.9. The contact angle of the silver PFBT-treated by vapor process is similar value of that by immersing process in PFBT solution (100 mmol/L). Therefore, this result indicates that the vapor process of SAMs is also valid to modify silver electrodes.

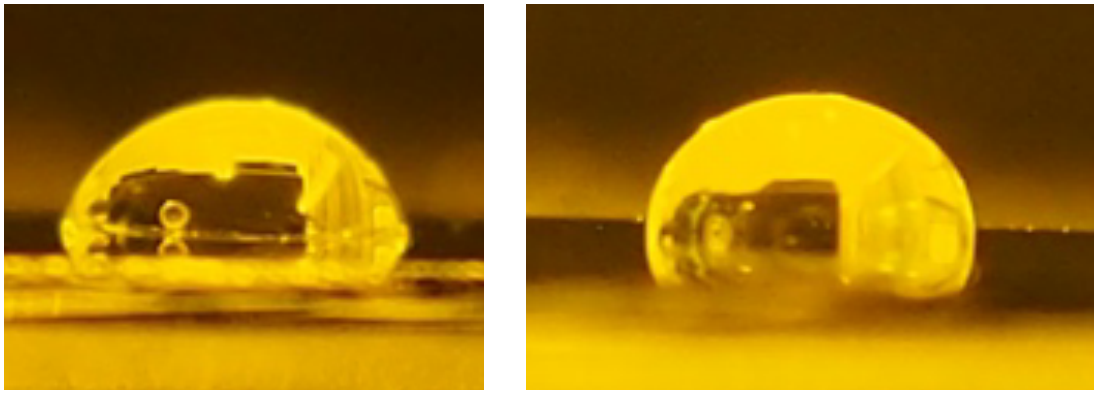

(a) (b)

Figure 4.9 Images of contact angle for (a) pristine silver and (b) PFBT-treated silver by vapor process.

4.3 OFET performance with silver S/D electrodes modified by several SAMs

OFETs with PFBT-modified silver S/D electrodes showed improved performance compared to OFETs with untreated silver S/D electrodes, however, it still exhibits large contact resistance because of the S-shape behaviour in low source/drain voltage in output characteristic as shown in Fig. 4.6. In order to achieve ideal output characteristics in low voltage, further approaches are required to investigate, and other SAM materials are being investigated. According to the research work by Mei et al. [15], 2,8-Difluoro-5,11-bis(triethylsilylethynyl) anthradithiophene (diF-TES ADT) OFETs with gold S/D electrodes modified with 4-(trifluoromethyl)-benzenethiol (TFBT: Fig. 4.10 (b)) and 2,3,5,6-tetrafluoro-4-(trifluoromethyl)-benzenethiol (TTFP: Fig. 4.10 (c)) showed improved performance compared to those with PFBT. Therefore, these SAMs materials have also been applied to Ph-BTBT-10 OFETs using silver electrodes. In this research, hence, two more SAM materials were prepared. One is pentafluorobenzenethiol (PFBT, Fig. 4.10(b)) well-known as a modifier of both gold and silver electrodes [12, 14, 15, 18-20]. The others are TFBT (Fig. 4.10 (b)) and 2,3,5,6-tetrafluoro-4-(trifluoromethyl)-benzenethiol (TTFP, Fig. 4.10(c)), and TTFP was newly applied to silver electrodes with Ph-BTBT-10 OFETs.

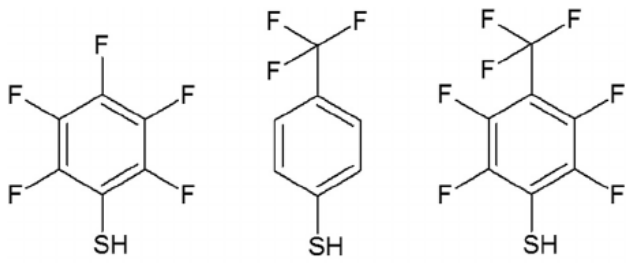

Figure 4.10 Chemical structures of SAM materials. (a) PFBT, (b) TFBT, and (c) TTFP.

Figure 4.11 shows transfer characteristics in the saturation region for Ph-BTBT-10 OFETs with untreated, TFBT-treated, PFBT-treated, and TTFP-treated silver S/D electrodes. OFETs with TFBT-treated silver exhibited better performance than those with untreated silver, however, worse performance than those with PFBT-treated silver. On the other hand, OFETs with PFBT-treated and TTFP-treated silver S/D electrodes showed about one order of magnitude increased drain current, as shown in Fig. 4.11(a). The mobility was extracted from the slope of transfer characteristics in the saturation region as shown in Fig.4.11(b). OFETs with the untreated silver S/D electrodes have low mobilities in the range of 10^{-2}-10^{-1} cm^2/Vs, and OFETs with TFBT-modified silver S/D electrodes also low mobility of 0.3 cm^2/Vs. While OFETs with PFBT-treated or TTFP-treated silver S/D electrodes exhibited mobility of about 1.5 cm^2/Vs. This result is an outstanding value since the mobility over 1 cm^2/Vs implies that the device can be utilized in applications for OLED displays. Therefore, in the following section, PFBT and TTFP will be discussed as SAM materials for silver electrodes.

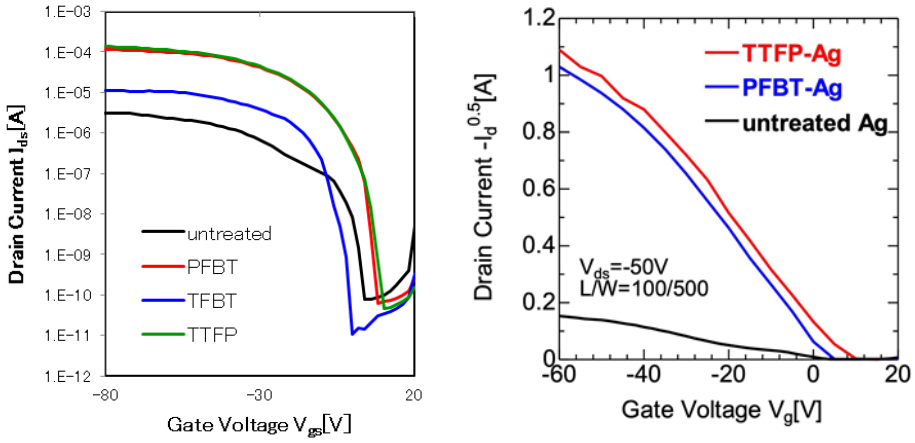

Figure 4.11 Transfer characteristics in the saturation region for Ph-BTBT-10 OFETs with untreated, PFBT-treated, TFBT-treated, TTFP-treated silver S/D electrodes.

Figure. 4.12 (a), (b), and (c) show the output characteristics of Ph-BTBT-10 OFETs with the untreated, PFBT-treated, and TTFP-treated silver S/D electrodes, respectively. Both OFETs with PFBT-treated and TTFP-treated silver S/D electrodes exhibited improved behaviour in the small drain voltage region, as shown in Fig. 4.12 (b) and (c), respectively. This result indicates SAM treatments led to the efficient injection of holes into the HOMO level of Ph-BTBT-10. Figure 4.12 (d) compared drain currents of OFETs with untreated, PFTB-treated, and TTFP-treated silver electrodes at low source-drain voltages at applied gate voltage of -20V. It is clear that both OFETs with PFBT-treated and TTFP-treated silver electrodes were excellent drain currents compared to OFETs with untreated silver electrodes. On top of that, it can be considered that OFETs with TTFP-treated silver electrodes showed slightly better performance than those of PFBT-treated silver electrodes.

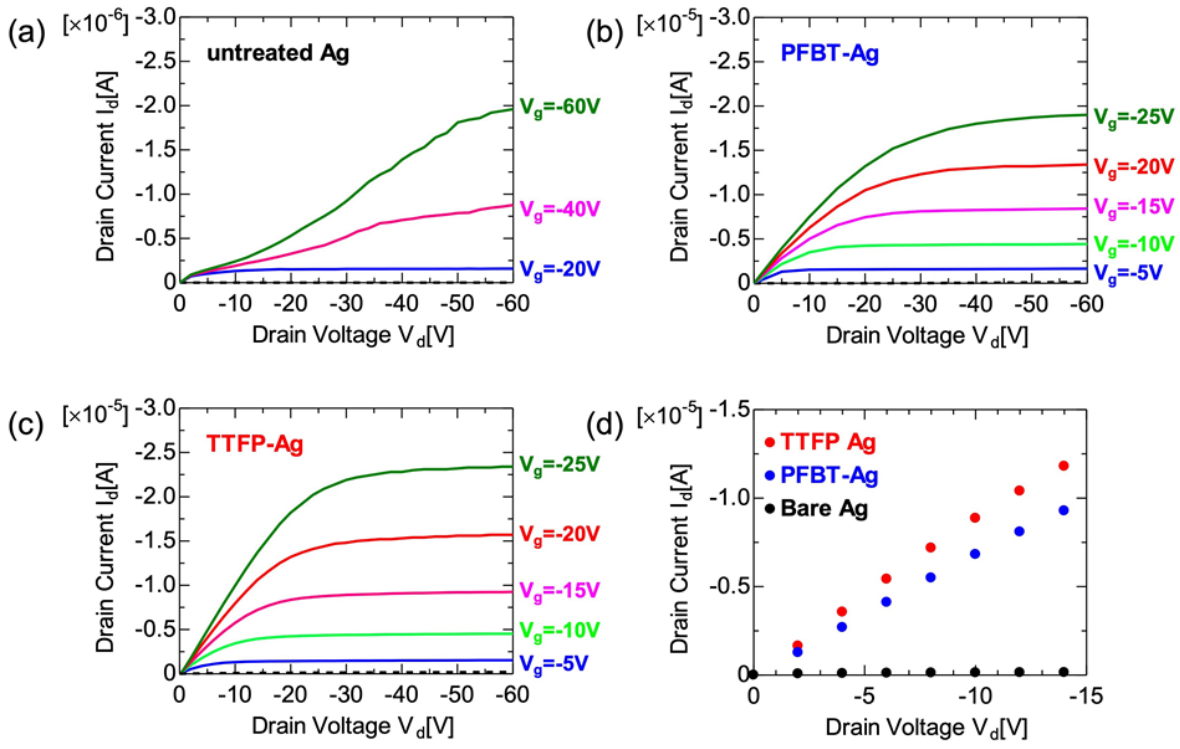

Figure 4.12 Output characteristics of Ph-BTBT-10 OFETs with (a) untreated, (b) PFBT-treate, and (c) TTFP-treated silver (Ag) S/D electrodes, and (d) comparison in small voltage

4.3.1 Contact resistance analyzed by transfer length method

The output characteristics of OFETs with SAMs-treated silver S/D electrodes are linear at low drain voltage and showed a well-defined linear to saturation transition, and these features denote small contact resistance and ohmic-like contact [3], [9]. For further analysis of contact resistance, TLM was used. Contact resistances are extracted from linear plots of R_{total} as a function of channel length as shown in Fig. 4.13 by obtaining the intersection with the y-axis. The obtained contact resistances of OFETs with PFBT-treated and TTFP-treated silver S/D electrodes were 3.9 kΩcm and 2.1 kΩcm, respectively. It exhibited two orders of magnitude lower than the contact resistances of OFETs with untreated silver S/D electrodes (630 kΩcm) as shown in Fig. 4.13 and Table 4.4. All contact resistance values exhibit at applied gate voltage, −60 V. These low contact resistances of OFETs with PFBT-treated and TTFP-treated silver S/D electrodes arise from the strong electron-withdrawing character of fluorine atoms presented in the SAMs. It creates a large internal dipole and when the dipole is directed from the organic semiconductor to the metal, the hole barrier height is reduced, that is, induces a work function of electrodes shifts downward [4]–[7].

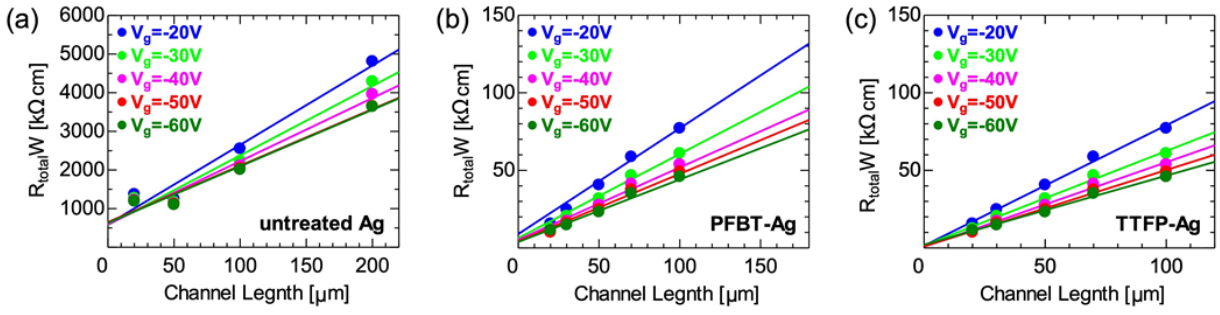

Figure 4.13 TLM results for Ph-BTBT-10 OFETs with (a) untreated, (b) PFBT-treated, (c) TTFP-treated silver (Ag) S/D electrodes.

Table 4.4 Electrical characteristics of Ph-BTBT-10 OFET with untreated, PFBT-treated, and TTFP-treated silver (Ag) S/D electrodes.

	Mobility [cm^2/Vs]	V_{th} [V]	R_c [kΩcm]
Untreated Ag	0.15	-8.8	630
PFBT-Ag	1.47	4.3	3.9
TTFP-Ag	1.51	6.4	2.1

4.3.2 Work functions of metals and HOMO level of Ph-BTBT-10

The work functions of untreated, PFBT-treated, and TTFP-treated silver electrodes were measured using photoelectron yield spectroscopy in the air (Riken keiki, AC-3), and Fig. 4.14 (a) shows the result. The work function of the untreated silver electrodes, 4.7 eV, has a large energy level misalignment with the HOMO level of Ph-BTBT-10, -5.5 eV in Chapter 3. However, this high hole injection barrier (~0.9 eV) was tuned by SAMs treatment with PFBT and TTFP respectively, resulting in ohmic-like contact in OFETs with silver S/D electrodes. The work functions of SAM-treated electrodes increased compared to untreated silver electrodes, and the work functions of PFBT-treated and TTFP-treated silver electrodes are measured to be 5.6 eV and 6.0 eV, respectively, as shown in Fig. 5 (a). Moreover, the work function of TTFP-treated silver electrodes shifted downwards more than the HOMO level of Ph-BTBT-10. This suggests that organic semiconductor materials with a deep HOMO level more than those of Ph-BTBT-10 (-5.5 eV) can also form ohmic contacts with lower charge injection barriers and contact resistance. In general, the device mobility of OFETs drops due to the contact resistance in short-channel [16], [17], still, Ph-BTBT-10 OFETs with TTFP-treated silver S/D electrodes did not drop mobility at short channel length (20 μm), as shown in Fig. 5 (b).

TTFP has a larger value of dipole moment than PFBT, thus, TTFP-treated silver electrodes were expected to have a high work function. In fact, TTFP-treated silver electrodes showed a deeper work function of 6.0 eV than that of PFBT-treated silver electrodes, and this energy level alignment indicated a reduction of contact resistance. Therefore, TTFP can be also one of the promising SAM materials for OFETs with silver electrodes. Moreover, since it has not yet been actively investigated its optimization condition, it has the potential possibility for improvement of OFETs performance.

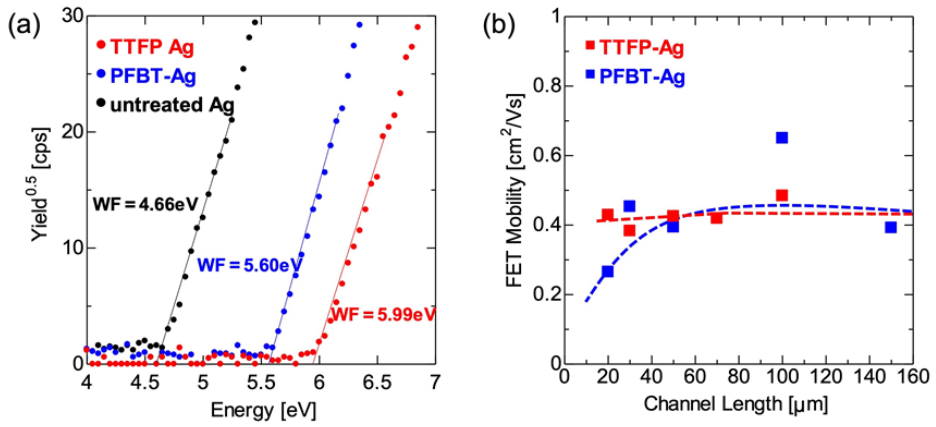

Figure 4.14 Work function of untreated, PFBT-treated, and TTFP-treated silver (Ag) electrodes evaluated by photoelectron yield spectroscopy in the air (a). Mobility of Ph-BTBT-10 OFETs with PFBT-treated and TTFP-treated silver S/D electrodes obtained from transfer characteristics in linear region as a function of channel length (b). Dash line is guide for the eye.

4.4 Conclusion and prospective

In this chapter, I have investigated interface engineering to enhance charge carrier injection in Ph-BTBT-10 OFETs with silver S/D electrodes by forming self-assembled monolayers. Ph-BTBT-10 OFETs with silver S/D electrodes in bottom-gate bottom-contact showed very low OFET mobility and high contact resistance because the work function of silver has a large energy level misalignment with the HOMO level of Ph-BTBT-10. SAMs-treated OFETs performances were remarkably improved exhibiting carrier mobility of about 1.5 cm^2/Vs. Contact resistances lowered by two orders of magnitude compared to OFETs with untreated silver S/D electrodes, and contact resistances of OFETs with PFBT- or TTFP-modified S/D electrodes were 3.9 kΩcm and 2.1 kΩcm, respectively. Also, TTFP-treated silver electrodes represented a high work function of 6.0 eV and showed no drop of mobility in short channel length. TTFP has not yet been actively investigated its optimization condition, so it is expected the potential possibility for improvement of OFETs performance. In conclusion, Ph-BTBT-10 OFET with SAMs-treated silver S/D electrodes is a promising candidate for high-performance low-cost OFETs.

References

[1] C. Di, Y. Liu, G. Yu, and D. Zhu, “Interface Engineering: An Effective Approach toward High-Performance Organic Field-Effect Transistors,” *Acc Chem Res*, vol. 42, no. 10, pp. 1573–1583, Oct. 2009.

[2] H. Ma, H. L. Yip, F. Huang, and A. K. Y. Jen, “Interface Engineering for Organic Electronics,” *Adv Funct Mater*, vol. 20, no. 9, pp. 1371–1388, May 2010.

[3] C. Liu, Y. Xu, and Y. Y. Noh, “Contact engineering in organic field-effect transistors,” *Materials Today*, vol. 18, no. 2, pp. 79–96, Mar. 2015.

[4] C. H. Kim et al., “Decoupling the Effects of Self-Assembled Monolayers on Gold, Silver, and Copper Organic Transistor Contacts,” *Adv Mater Interfaces*, vol. 2, no. 2, Jan. 2015.

[5] H. Kim, Z. Meihui, N. Battaglini, P. Lang, and G. Horowitz, “Large enhancement of hole injection in pentacene by modification of gold with conjugated self-assembled monolayers,” *Org Electron*, vol. 14, no. 9, pp. 2108–2113, Sep. 2013.

[6] J. C. Love, L. A. Estroff, J. K. Kriebel, R. G. Nuzzo, and G. M. Whitesides, “Self-assembled monolayers of thiolates on metals as a form of nanotechnology,” *Chem Rev*, vol. 105, no. 4, pp. 1103–1169, Apr. 2005.

[7] S. Khodabakhsh et al., “Using self-assembling dipole molecules to improve hole injection in conjugated polymers,” *Adv Funct Mater*, vol. 14, no. 12, pp. 1205–1210, Dec. 2004.

[8] J. Roh et al., “Injection-modulated polarity conversion by charge carrier density control via a self-assembled monolayer for all-solution-processed organic field-effect transistors,” *Scientific Reports* 2017 7:1, vol. 7, no. 1, pp. 1–8, Apr. 2017.

[9] J. P. Hong, A. Y. Park, S. Lee, J. Kang, N. Shin, and D. Y. Yoon, “Tuning of Ag work functions by self-assembled monolayers of aromatic thiols for an efficient

hole injection for solution processed triisopropylsilylethynyl pentacene organic thin film transistors," *Appl Phys Lett*, vol. 92, no. 14, 2008.

[10] H. Y. Chen, I. W. Wu, C. T. Chen, S. W. Liu, and C. I. Wu, "Self-assembled monolayer modification of silver source–drain electrodes for high-performance pentacene organic field-effect transistors," *Org Electron*, vol. 13, no. 4, pp. 593–598, Apr. 2012.

[11] K. Aoshima, S. Arai, K. Fukuhara, T. Yamada, and T. Hasegawa, "Surface modification of printed silver electrodes for efficient carrier injection in organic thin-film transistors," *Org Electron*, vol. 41, pp. 137–142, Feb. 2017.

[12] K. D. Jung et al., "A study on the carrier injection mechanism of the bottom-contact pentacene thin film transistor," *Appl Phys Lett*, vol. 96, no. 10, Mar. 2010.

[13] S. Chung, J. Jeong, D. Kim, Y. Park, C. Lee, and Y. Hong, "Contact resistance of inkjet-printed silver source-drain electrodes in bottom-contact OTFTs," *J. Disp. Technol.*, vol. 8, no. 1, p. 48, 2012.

[14] D. Meyer et al., "Dithiocarbamate Self-Assembled Monolayers as Efficient Surface Modifiers for Low Work Function Noble Metals," *Langmuir*, vol. 32, no. 35, pp. 8812–8817, Sep. 2016.

[15] Y. Mei et al., "Interface engineering to enhance charge injection and transport in solution-deposited organic transistors," *Org Electron*, vol. 50, pp. 100–105, Nov. 2017.

[16] M. Marinkovic, D. Belaineh, V. Wagner, and D. Knipp, "On the origin of contact resistances of organic thin film transistors," *Adv. Mater.*, vol. 24, no. 29, p. 4005, Aug. 2012.

[17] Y. Shi, J. Liu, Y. Hu, W. Hu, and L. Jiang, "Effect of contact resistance in organic field-effect transistors," *Nano Select*, vol. 2, no. 9, pp. 1661–1681, Sep. 2021.

Chapter 5
Study on OFETs using solution-processed silver S/D electrodes

5.1 Introduction

Ph-BTBT-10 thin film transistors with silver S/D electrodes are a promising candidate for next-generation organic devices, showing outstanding performance. Performances of the top contact OFETs were comparable or superior to those with gold S/D electrodes despite the bigger energy level mismatch as shown in Chapter 3. Also, performances of the bottom contact OFETs with SAMs-modified silver S/D electrodes showed mobility of over 1 cm^2/Vs as shown in Chapter 4. It is expected that organic electronics to provide eco-friendly, large-area, and ultra-low-cost manufacturing for flexible device applications [1]–[5]. By applying fabrication processes based on printing with silver nanoparticles ink to these research achievements, it is expected the realization. In this chapter, therefore, solution-processed silver S/D electrodes will be investigated. First, the inkjet printing process which has the merit of ultra-low-cost and reduction of process time by the drop-on-demand method will be demonstrated. The second approach of the solution process is coated silver nano-ink utilizing differential hydrophobic and hydrophilic surface properties. By using silver nanoparticles, I aim at ultra-low-cost and high-performance OFETs: both active layer and S/D electrodes fabricated by solution processes without vacuum evaporated process, which requires high vacuum pressure and temperature, it is also expected to be eco-friendly and reducing the process time and steps.

5.2 Inkjet-printed silver electrodes

In order to realize ultra-low-cost OFETs, it is one of the promising methods to fabricate S/D electrodes by inkjet printing technology, since it can reduce the fabrication processing time and enable us to get patterned electrodes on the large area, simply and easily [1], [2]. Therefore, Ph-BTBT-10 thin film transistors with solution processed silver S/D electrodes by inkjet printing is investigation, which has the merit of ultra-low-cost and reduction of process time by the drop-on-demand method I selected the silver nanoparticles which are dispersion in the hydrocarbon organic solvent, tetradecane, NPS-L is provided by Harima Chemicals, Inc. The silver nanoparticles paste, NPS-L, were synthesized for inkjet printing. In the case of top contact configuration, there are mainly two problems to fabricated S/D electrodes by using inkjet printing. Because a relatively high-temperature sintering process is required for the printed S/D electrodes and ink solvent can damage the bottom layer, especially the semiconductor layer, when S/D electrodes are printed at the end of the OFET fabrication process. Therefore, their electrical contact performance is generally poor in comparison with OFETs that are typically fabricated by the conventional vacuum process. However, in the case of the silver nano paste provided by Harima Chemicals, Inc., the sintering temperature is over 120 ℃, and it matches Ph-BTBT-10 thermal annealing temperature, so I investigated how much ink solvent damage Ph-BTBT-10 semiconductor layer in top contact. Moreover, I fabricated silver nano paste on SiO_2/Si substrate by inkjet printing for bottom contact configuration.

5.2.1 Silver patterning in top contact structure by inkjet printing

In order to check that ink solvent (tetradecane) damages the semiconductor, I investigated the silver paste fabricated by inkjet printing on Ph-BTBT-10 semiconductor layer and sintering the silver by heating. In this experimental, the SiO_2/Si substrates are cleaned by ultrasonic

cleaner. And Ph-BTBT-10 semiconductor layer was fabricated by spin coated 0.45wt% or 0.7wt%, *p*-xylene solution with 3000 rpm for 30 s. And dot patterns of silver paste were fabricated by inkjet printing on the Ph-BTBT-10 semiconductor layer. The substrates are heated at 45 °C in order to dry the solvent of silver paste as quick as possible. And then, the substrates were heated at 120 °C for 1 hour by hot plate.

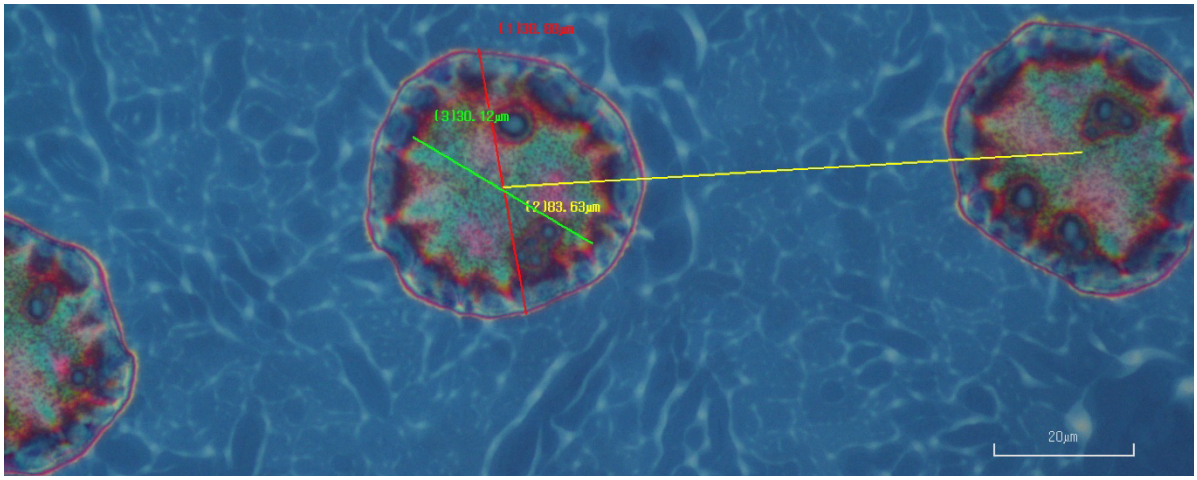

(a)

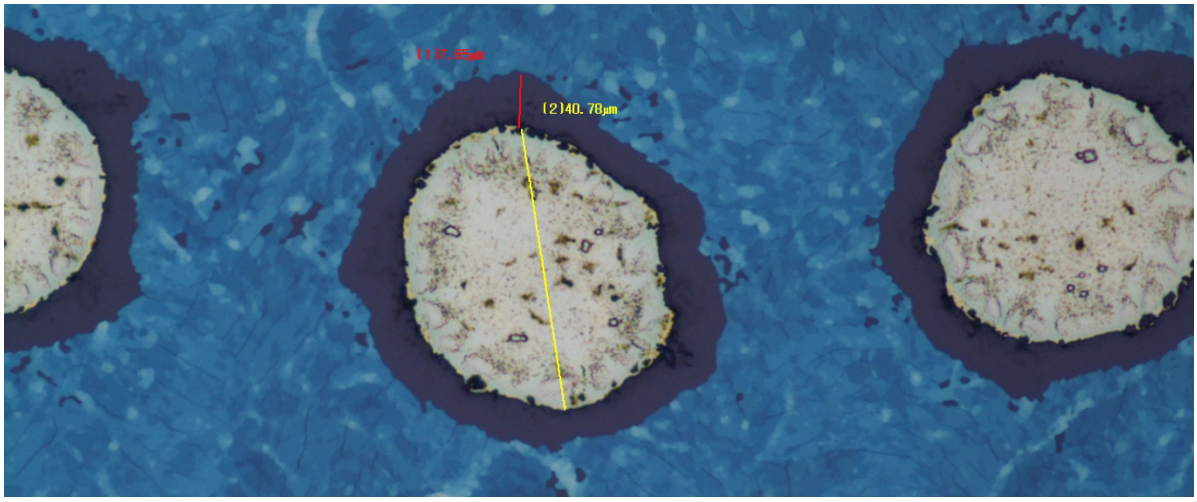

(b)

Fig. 5.1 Image of inkjet printed silver dot. Drop spacing is 80 μm and Ph-BTBT-10 semiconductor layer was fabricated by 0.45 wt% *p*-xylene solution. (a) Before and (b) after sintering by heating at 140 °C for 1 hour.

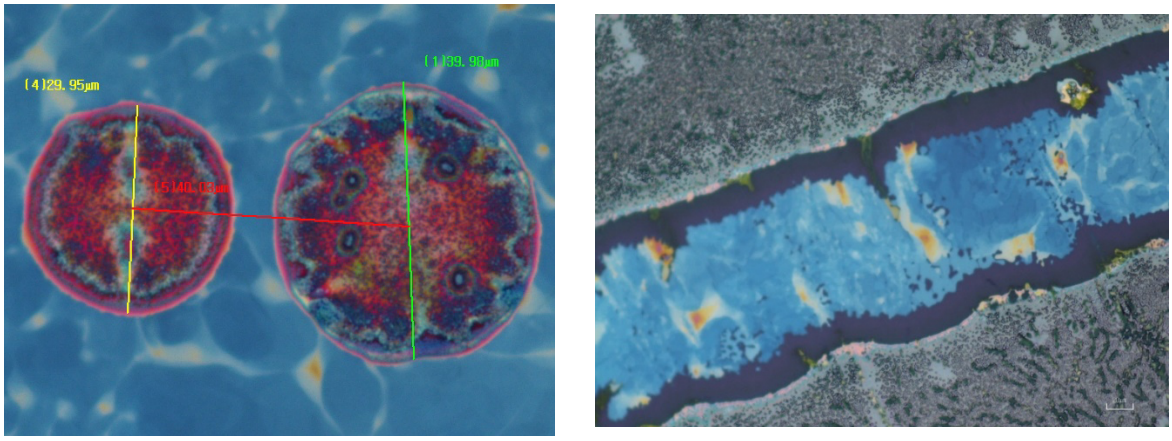

(a) (b)

Fig. 5.2 Image of inkjet-printed silver (a) dot and (b) line. Ph-BTBT-10 semiconductor layer were fabricated 0.7 wt% *p*-xylene. (a) Before and (b) after sintering by heating at 140 °C for 1 hour.

As shown in Fig. 5.1 (a), the Ph-BTBT-10 semiconductor layer was not damaged before sintering, which indicated that the hydrocabone solvent of silver nano paste, tetradecane, is low solubility for Ph-BTBT-10 and does not damage Ph-BTBT-10 thin layer. However, the Ph-BTBT-10 semicondcutor layer around silver ink dot was destroyed after sintering at 140 °C for 1 hour as shown in Fig. 5.1(b). There were no significant changes for diferrence Ph-BTBT-10 film thickness, which is fabricated with between 0.45 wt% and 0.7 wt% *p*-xylene solution as shown in Fig. 5.2. Therefore, it can be concluded that silver nano paste ink was not proper to fabricate top contact OFETs. To fabricate top configuration OFTEs, it is required to consider other ink which is not to damage the semiconductor layer after sintering.

5.2.2 Silver electrode by inkjet printing for bottom contact structure

In top contact configuration, silver nano paste with organic solvent, tetradecane, did not dissolved Ph-BTBT-10 semiconductor layer, however, sintering process at 140 °C for 1 hour damage Ph-BTBT-10 semiconductor layer. On the other hand, patterning silver nano paste and sintering process do at first in bottom contact configuration before the fabrication of Ph-BTBT-10 semiconductor layer. Bottom contact configuration is suitable structure for the fabrication

of printed source and drain electrodes.

I investigated the critical parameter for pattering electrodes by inkjet printing and to confirm these parameters I fabricated a dot pattern using silver nano paste ink for bottom configurations. I make hypothesis critical parameter for making fine source/drain electrode pattering. The surface condition of substrate control diffusion of silver nano paste, highly wettability of surface condition by treatment suppress diffusion of silver nano paste before drying silver nano particles. It is important to control the speed of volatilization of organic solvent, tetradecane. The control of the temperatures such as stage of ink jet printer is important to suppress the flow of the ink droplet (bulge).

SiO_2/Si substrates were cleaned using ultrasonic cleaner. Dot patterns were fabricated by inkjet printer. The stage temperature of inkjet printer hold at 45 ºC. And then, in order to sinter the silver nano paste, the samples were heated on the hot plate at 120 ºC for 1 hour.

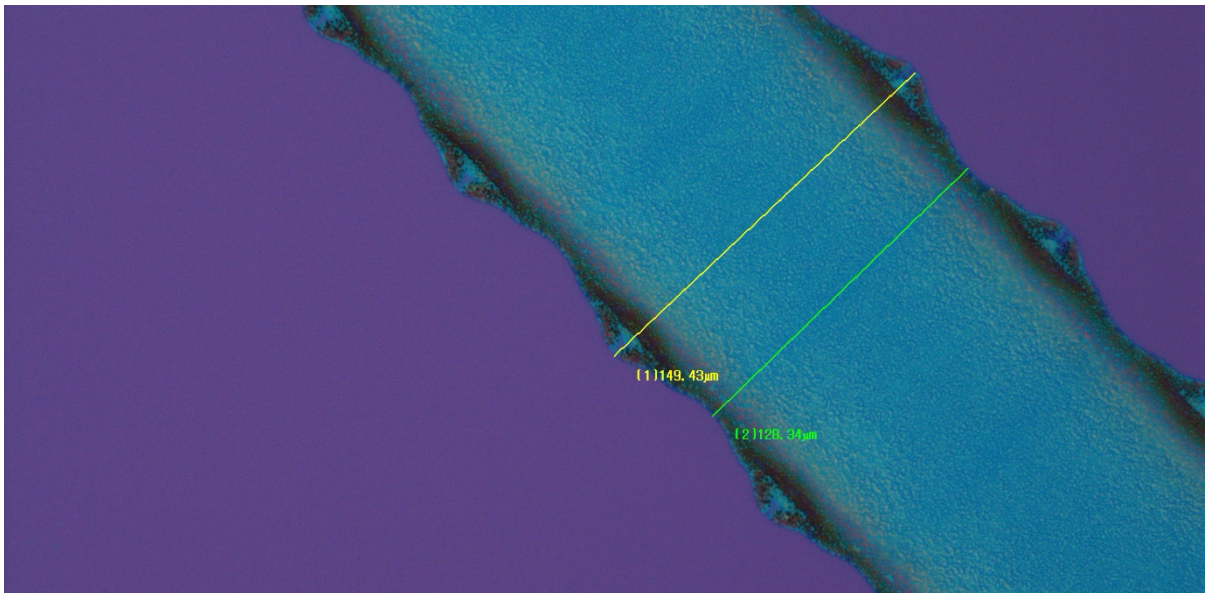

(a)

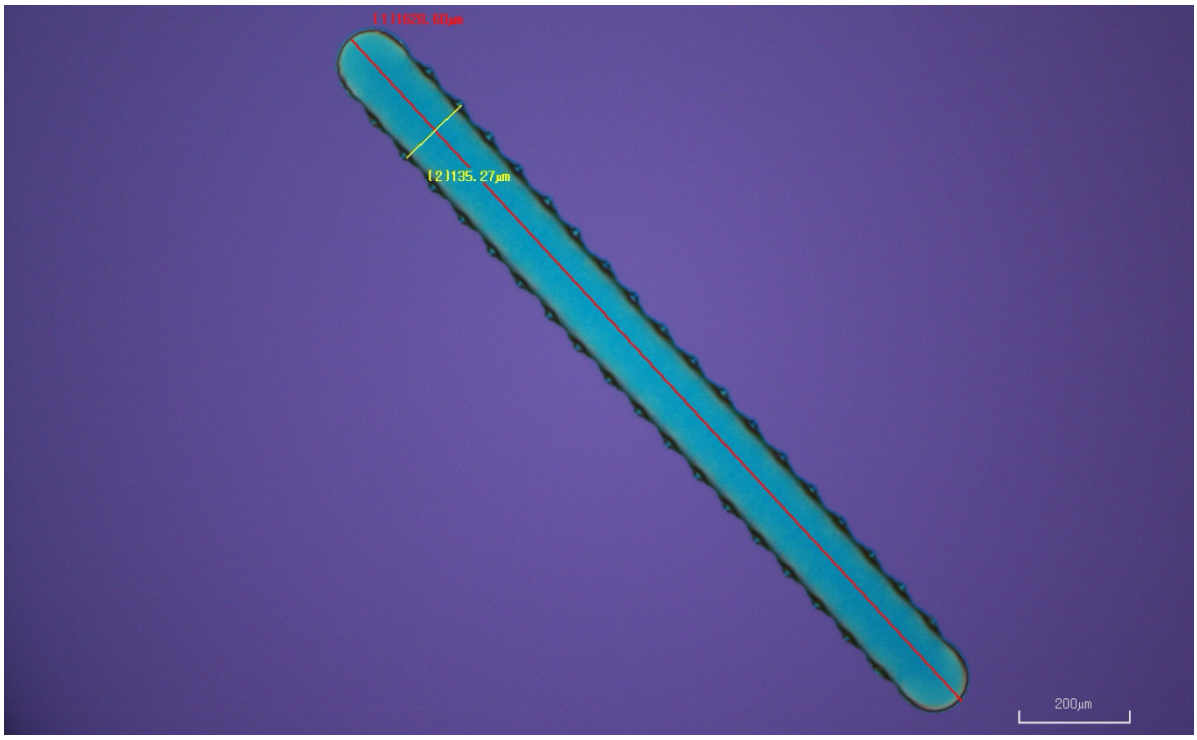

(b)

Figure 5.3 Images of inkjet-printed silver dot before sintering. Drop spacing is 100 μm and the number of dot is 17.

Compared to the top-contact structure, there are significant differences. For the top contact configuration, it was not overlapped even though when drop spacing is 40 μm as shown in Fig. 5.1, on the other hand, for the bottom-contact structure when drop spacing was 100 μm dot patterns were overlapped. The result of drop spacing 135 μm showed unoverlapped dot. Also, dot size exhibited a big difference. Dot sizes show about 40 μm and about 130 μm on the Ph-BTBT-10 semiconductor layer and SiO_2/Si, respectively. Therefore, it can be concluded that dot size is greatly affected by the underlayer condition. Surface treatment can be a possible solution to fine patterns.

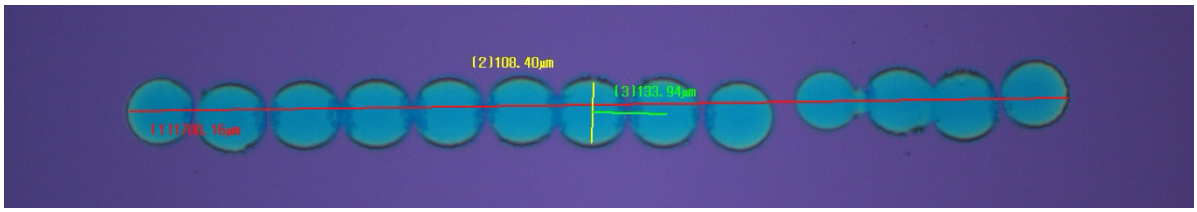

(a)

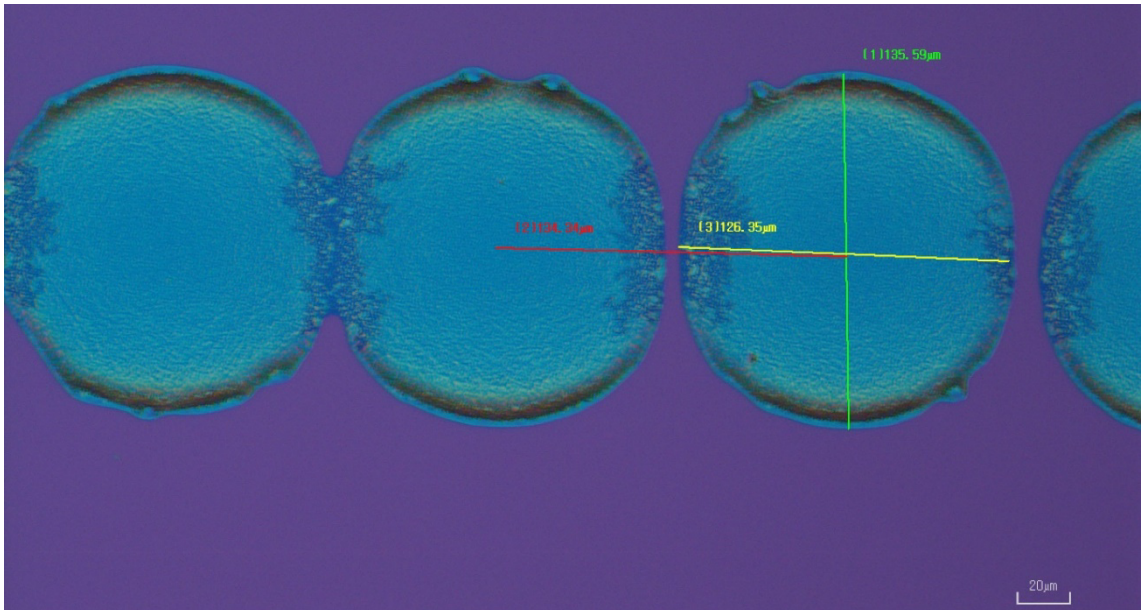

(b)

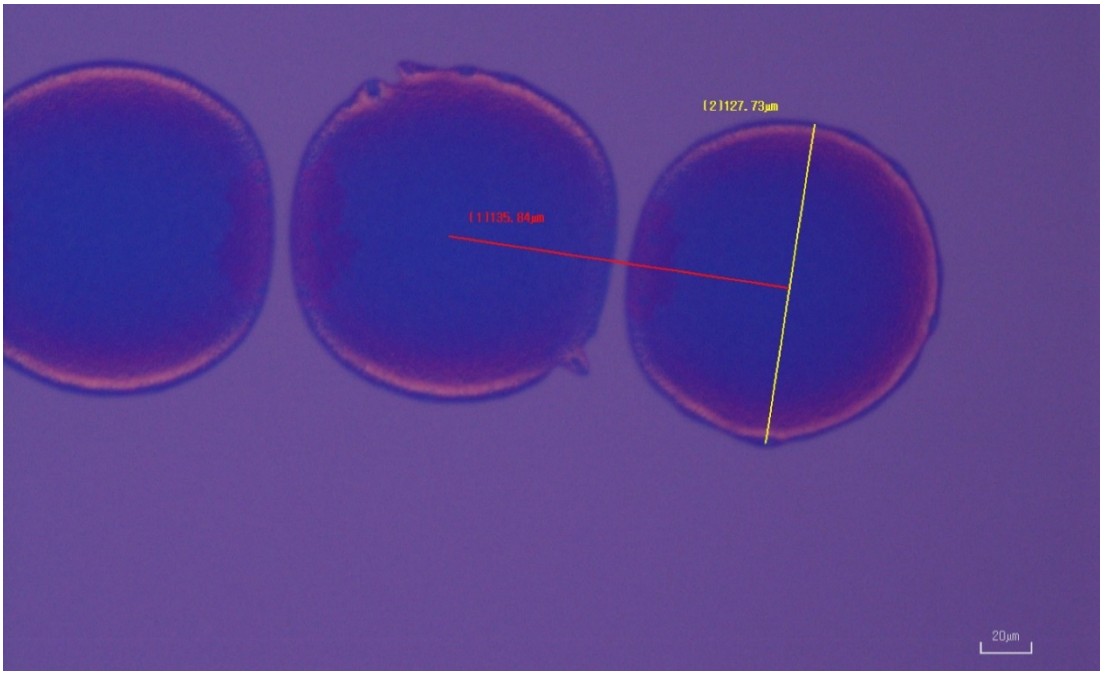

(c)

Figure. 5.4 Images of inkjet-printed silver dot (a, b) before and (c) after sintering. Drop spacing is 135 μm and the number of dot is 13.

5.2.3 Conclusion and Challenges of Inkjet printing

For the INKJET PRINTING process, relatively non-wavy dot line patterns were obtained by adjusting the condition between Silver Nanoparticle and surface, the detail is explained as shown in Fig. 5.5. Therefore, the next step is the fabrication of OFETs, and then evaluate and compare to the conventional process. Furthermore, to improve the properties and get fine pattern various underlayer will be applied because through the previous investigation it is clarified that the Silver Nanoparticle is greatly affected by the underlayer condition. However, it is difficult to control the fabrication condition and fine pattern. It is because that the goal of this research is the fabrication of high-performance OFETs by solution process, not only inkjet printing process. Therefore, the second approach of the solution process is spin coating Silver Nanoparticle utilizing differential hydrophobic and hydrophilic surface properties.

Figure. 5.5 Schmatic isslustration of drop size on hydrophobic and hydrophilic surface of Ph-BTBT-10 semiconductor layer and SiO_2/Si substrate, respectively.

5.3 Printed silver electrode using differential surface energy

In order to improve the performance of OFETs with inkjet-printed silver electrodes, a number of research groups have exerted effort, however, it is difficult to achieve fine patterns directly using only inkjet printing methods. Recently, some groups have suggested new solution processes with the consideration of the differential surface wettability to fabricate fine patterns [6]–[9]. In this section, therefore, to manufacture fine silver S/D electrode patterns, the approach of the solution process using differential hydrophobic and hydrophilic surface properties is applied. So as to realize the hydrophobic and hydrophilic surface pattern, several concepts were considered and three methods will be introduced in this section: hydrophobic anc hydrophilic self-assembled monolayers, fluorinated polymer using O_2 plasma, and photoreactive self-assembled monolayers.

5.3.1 Concept 1: patterning using self-assembled monolayers and dry etching

First of all, the gate dielectric self-assembled monolayers (SAMs) materials were considered in order to form the hydrophobic and hydrophilic patterns, which is a very simple and easy process. The silver nanoparticle ink used in this section is NPS-L (Harima Chemical), which was used for inkjet printing. The silver nanoparticle ink NPS-L can be controlled by hydrophobic and hydrophilic properties as shown in the former section, and Sugino et al reported the fine patterns of silver S/D electrodes with Harima silver nanoparticle ink [9]. Therefore, NPS-L ink is considered a feasible candidate for this differential surface energy concept. The concept of the SAMs patterning process for the silver S/D electrode was demonstrated in Fig. 5.6. First, it is required to fabricate a hydrophobic layer on the Si/SiO_2 substrates and dodecyltriethoxysilane (DTS), well-known for one of the SAMs materials for the gate dielectric layer, was used. It was drop-casted on the hot plate and covered by a petri dish, then evaporated at 140 ℃ for 40 minutes. Next, substrates were placed on a magnetic

plate, and metal shadow masks were magnetically adhered to the substrates, exposing the designated area for the formation of electrodes. DTS was oxidized by ozone of UV/O_3 cleaner for 20 minutes. In this process, DTS was removed exposing the SiO_2 layer, thus, the designated area for the formation of electrodes has relatively hydrophilic properites. Then, phenyltriethoxysilane (PTS), one of the SAMs materials exhibiting hydrophilicity [10], was drop-casted and evaporated by covered with a petri dish at 140 ℃ for 40 minutes, to strengthen hydrophilic properties in designated areas for the formation of electrodes. It was tried to form silver S/D electrodes using silver nanoparticles (NPS-L) by blade coating, however, the silver nanoparticles were uniformly coated the whole area on Si/SiO_2 substrates not to pattern. It was considered that the surface energy was not strong enough to pattern silver electrodes.

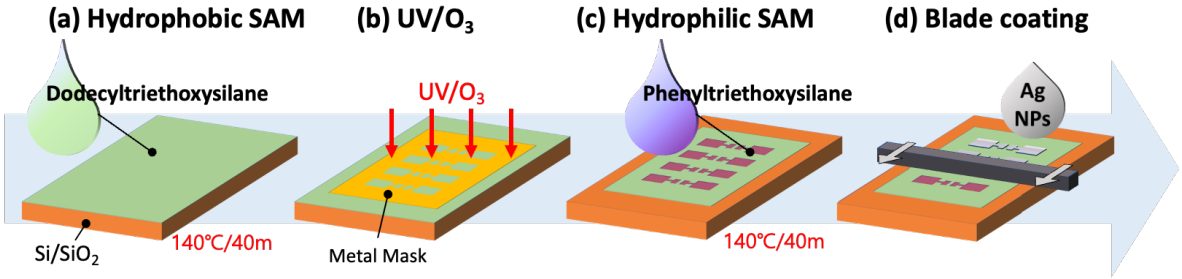

Figure. 5.6 Conceptual illustration of the patterning process using differential surface energy with the hydrophobic and hydrophilic SAMs materials dodecyltriethoxysilane (DTS) and phenyltriethoxysilane (PTS), respectively. (a) DTS was drop-casted. (b) DTS was oxidized by exposure to UV light in an ozone atmosphere. (c) PTS was drop-casted. (d) Silver nanoparticles (AgNPs) ink was blade coated.

5.3.2 Concept 2: Pattering using fluorinated polymer and dry etching

Differential surface wettability formed by the gate dielectric SAM materials with DTS and PTS was not enough to form the silver S/D electrode patterns, therefore, intensifying hydrophobic properties of the underlayer can be applied. The fluorinated polymer, CYTOP, has hydrophobic properties and can be fabricated by solution process. CYTOP is known to be very hydrophobic with a water contact angle of ~110° and cannot be detached from the substrate by water and

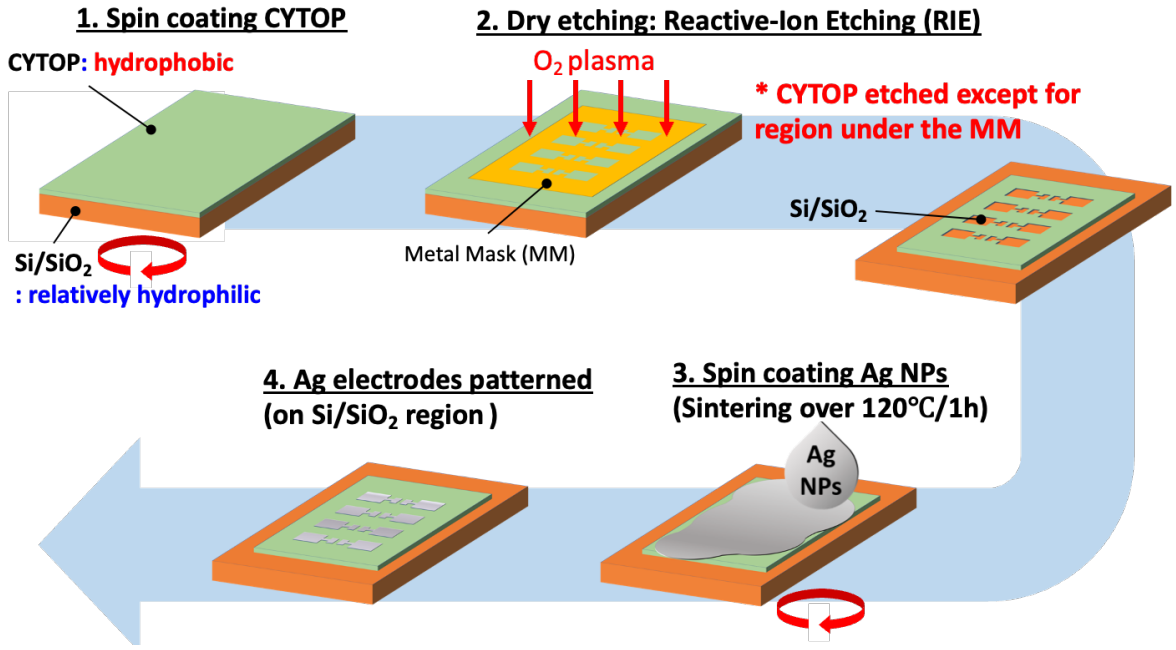

Figure. 5.7 Conceptual illustration of the patterning process for the silver electrode spin-coated onto a selectively treated surface. (a) The underlayer and hydrophobic CYTOP were spin-coated. (b) The CYTOP was patterned by dry etching using reactive-ion etching. (c) Silver nanoparticle ink was spin coated.

organic solvents, such as chloroform, acetone, and toluene [11]–[13]. Also, CYTOP patterning can be simply achieved through dry etching with a metal shadow mask because the C–F bonds in the CYTOP are broken by O_2 plasma. Therefore, in this section, CYTOP was selected as an underlayer to fabricate a hydrophobic surface. Fig. 5.7 shows the conceptual illustration explaining the patterning process for the silver electrode spin-coated on a selectively treated surface. The first step is spin coating CYTOP on the Si/SiO_2 substrates to form a hydrophobic underlayer. CYTOP solution was prepared to 1:3 complex CYTOP and its solvent, CT-solv180. CYTOP solution was spin-coated at 2000 rpm for 60 seconds and the CYTOP layer was cured by baking at 90 ℃ for 20 minutes with glass sealed condition. Then, the CYTOP layer was dry etched by O_2 plasma using reactive-ion etching (RIE). It was also magnetically adhered to the substrates with a metal shadow mask expositing the designated area for S/D electrodes. As shown in Fig. 5.8(a), fine etched patterns can be obtained: sky blue represents the area that

remains CYTOP and violet represents the area that SiO_2 was exposed. CYTOP has hydrophobicity, whereas the exposed region was revealed SiO_2, which has relatively hydrophilic properties and well-wettable for the solution. These differential surface properties can allow silver nanoparticles to be coated only on the SiO_2 surface by spin-coating. After fabricating electrodes, it is sintered over 120 ℃ for 1 hour. As shown in Fig. 5.8 (c), relatively well-patterned electrodes were achieved in the first trials. However, it was lack of reproducibility of patterned silver S/D electrodes. Most of patterns were exhibited such as Fig. 5.8 (b). To improve reproducibility, it is needed to optimize the condition of spin-coating of silver nanoparticle ink and the thickness of CYTOP.

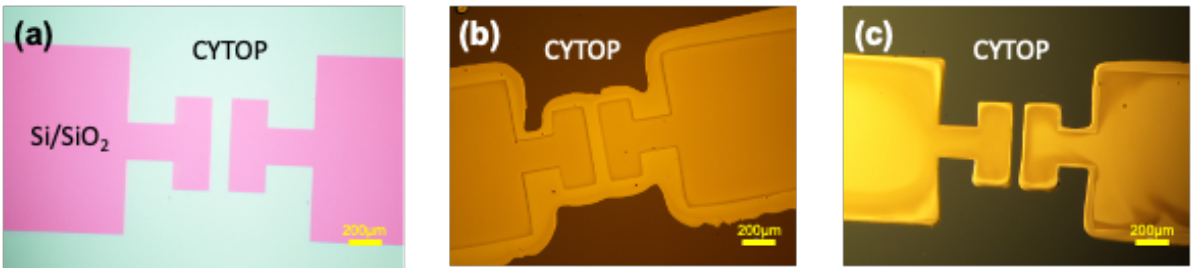

Figure 5.8 Optical images (a) patterned CYTOP and (b) (c) patterned silver fabricated by spin coating using diffrential surface energy with CYTOP layer and dry etching. (b) Average pattern and (c) Best pattern.

5.3.3 Challenges of organic solvent and water type silver inks

As mentioned in the former section, the reproducibility of fabricating silver electrodes was very poor. It is considered that the patterning of silver electrodes using silver nanoparticles NPS-L, Harima, is more affected by the thickness gap between the CYTOP layer and Si/SiO_2 layer, rather than the differential surface energy of hydrophilic and hydrophobic. Figure 5.9 illustrated that the silver nanoparticles ink was confined in the CYTOP-etched area due to the step between CYTOP and SiO_2. Therefore, the hydrophilicity of silver nanoparticles was also considered in order to intensify the differential surface energy. The newly employed silver nanoparticle ink, synthesized and provided by Bando Chemical Industries, Ltd, is dispersed in

glycerin and water. It has more hydrophilic properties than organic solvents of NPS-L. Figure 5.10 showed the patterns of solution-processed silver S/D electrodes as different silver nanoparticles inks, Harima and Bando, respectively. Red dashed lines are a guide for a designated area for the formation of S/D electrodes. The silver electrode pattern with Bando silver ink appeared fine pattern (Fig. 5.10 (c)) while the silver electrode pattern with Harima silver ink spread out the red line (Fig. 5.10 (b)). As a result, by stregnthen the hydrophilic properties of the silver nanoparticle ink with Bando silver ink, fine patterned silver S/D electrodes were achieved using the CYTOP layer patterned by O_2 plasma, in addition, it did not require the formation of the thicker CYTOP layer.

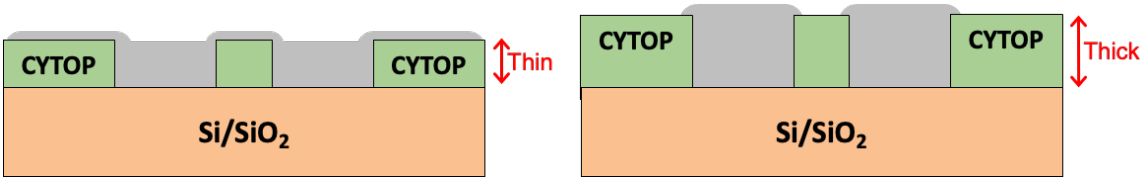

Figure 5.9 Conceptual illustration of the patterning process for the silver electrode spin-coated onto a selectively treated surface.

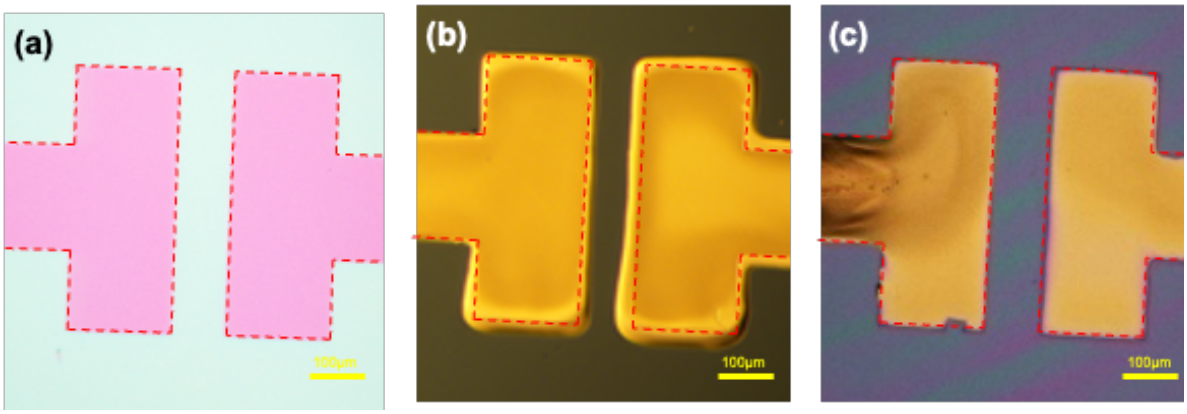

Figure 5.10 Optical images of (a) paternd CYTOP, and silver electrodes which were fabricated by (b) silver ink dispersed in tetradecane, Harima and (c) silver ink dispersed in water and glycerin, Bando. Red dashed lines are a guide for a designated area for the formation of S/D electrodes.

5.3.4 Cocept 3: pattering using photoreactive self-assembled monolayer

Photoreactive self-assembled monolayers can be a good alternative for the issue of the underlayer thickness since it is very thin. In this section, therefore, the method of photo-patterning without using a resist was investigated. In this section, Bando silver nanoparticle ink was used. As stated in Chapter 2, these hydrophobic photoreactive SAM-treated substrates were provided by Nikon Corporation, and the photoreactive SAM is composed of amino groups and photoresponsive protecting groups. Photoresponsive protecting groups have hydrophobic properties and after UV exposure, the protective group was decomposed and eliminated. Thus, the suppressed performance of amino groups is activated and it has hydrophilic properties as shown in Fig. 5.11. UV exposure was conducted using a mask aligner. Metal shadow masks were magnetically adhered to the substrates, and the designated area for S/D electrodes was only exposed. After exposure, to remove the residue of SAM it was rinsed with chloroform, and then cleaned with isopropyl alcohol (IPA) by an ultrasonic cleaner for 3 minutes. So the exposed area has hydrophilic properties and fine silver S/D electrode patterns can be easily obtained by both spin coating and blade coating. Fig. 5.12 shows the optical images of the blade coating with squeegees, the channel length of 10 μm was also successfully fabricated.

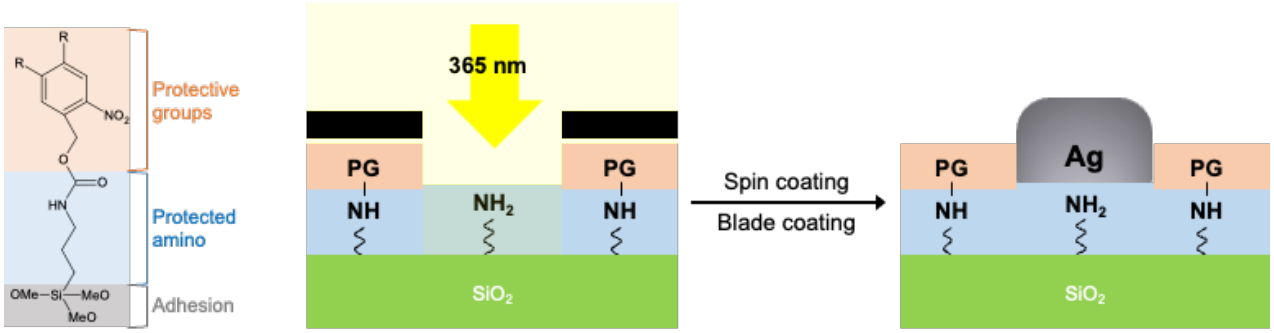

Figure 5.11 Concept issulstration of photoreactive self assemly monolaeyr

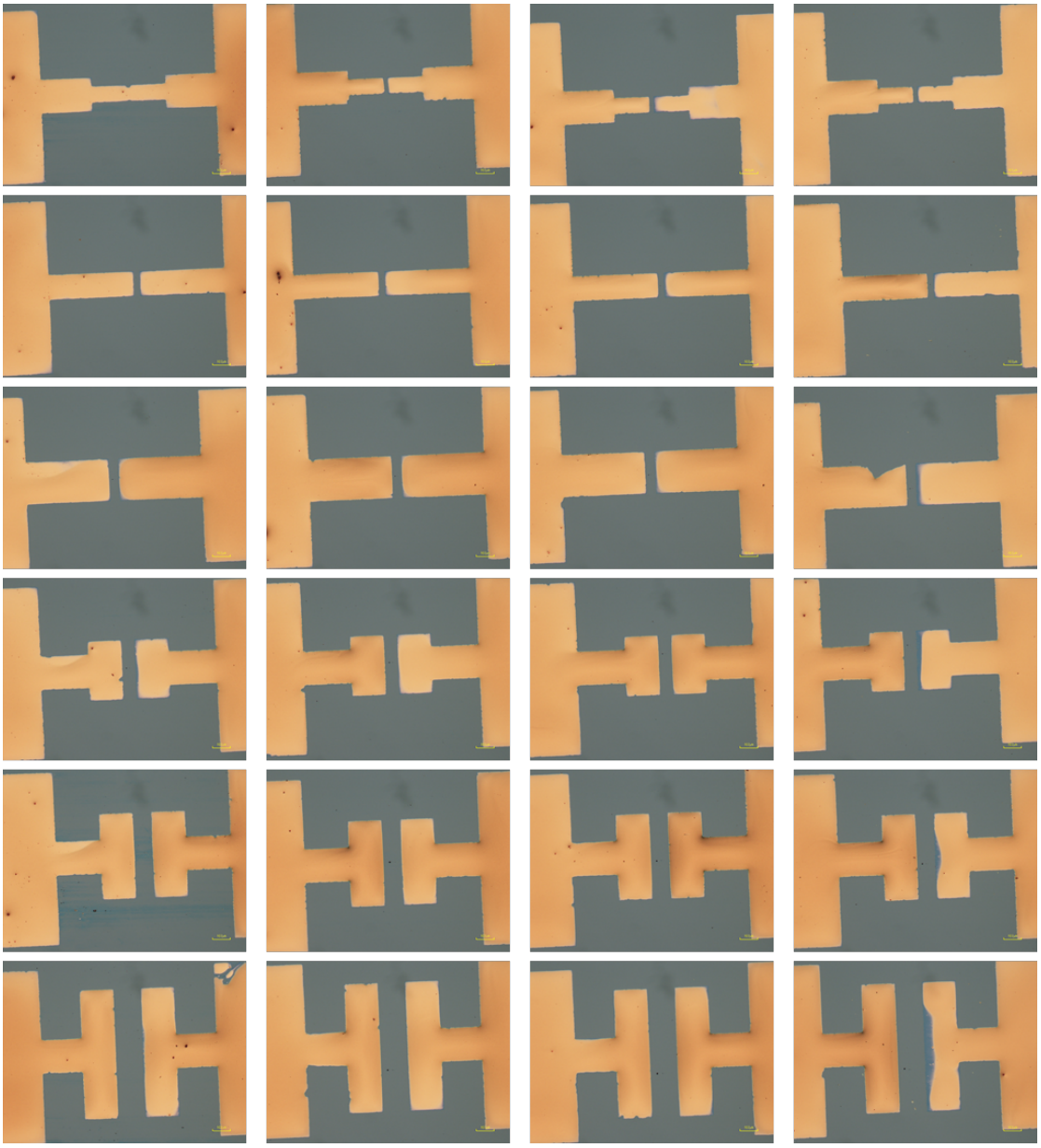

Figure 5.12 Optical images of photo patterning silver electrodes

5.3.5 Challenges of Ph-BTBT-10 thin film formation

By the concept of the CYTOP layer using O_2 plasma, fine silver S/D electrodes were achieved. However, there were some issues with the formation of Ph-BTBT-10 thin-film. The CYTOP residue is hard to form Ph-BTBT-10 onto the CYTOP layer due to its thickness or hydrophobic properties. The CYTOP layer thickness is quite thick tens of nanometers, even though it is successfully fabricated thin enough, and the hydrophobicity is so strong that Ph-BTBT-10 cannot be spin-coated on the CYTOP layer. Therefore, the residue of CYTOP on the

channel area must be removed. When the silver S/D fabricated substrates were fully etched by using O_2 plasma, it sometimes damaged silver S/D electrodes, so the reproducibility was unstable to fabricate OFETs. So further investigation is required.

For the silver S/D electrodes patterned by the photoreactive SAMs, as the same with the CYTOP process, the channel area is hydrophobic so without no additional treatment it is difficult to fabricate Ph-BTBT-10 thin film as shown in Fig. 5.13 (a). However, for the photoreactive SAMs, as exposed after fabricating silver S/D electrodes, photoreactive protecting groups on the channel area can be removed, and additional UV/O_3 cleaning improves the uniform formation of Ph-BTBT-10 thin film, as shown in Fig. 5.13 (b). As a result, Ph-BTBT-10 OFETs with solution-processed silver S/D electrodes were successfully fabricated and operated.

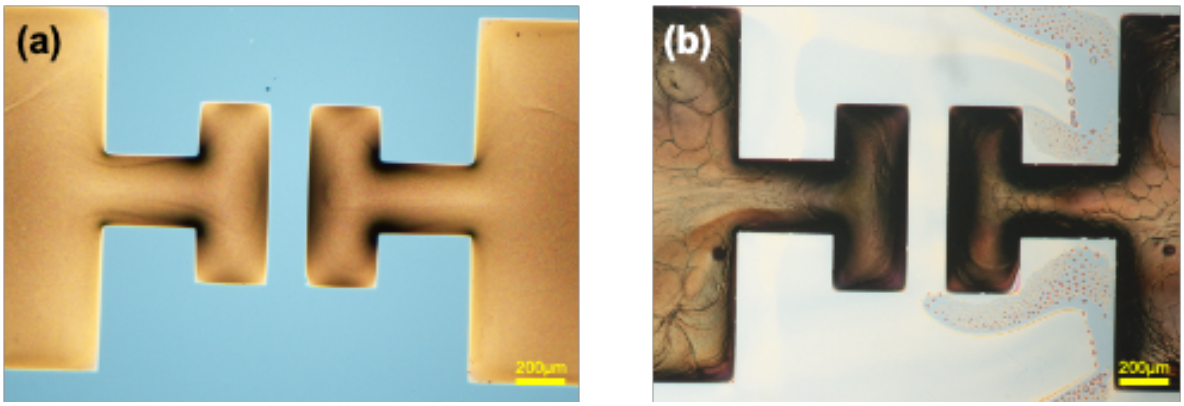

Figure 5.13 Characteristics of OFETs with photo pattering Ag electrodes modified with TTFP

5.4 OFETs with solution processed silver electrodes

First, to confirm whether the devices operate or not, OFETs without any treatment in silver electrodes were fabricated and evaluated. Figure 5.14(a) showed the characteristics of Ph-BTBT-10 OFET with solution-processed pristine silver electrodes by photo patterning. Even though it exhibited a very low OFET mobility in the range of 10^{-3} cm^2/Vs, this is the first achievement for Ph-BTBT-10 thin-film transistors with solution-processed silver S/D electrodes. Figure 5.14(b) showed the characteristics of those with modified silver electrodes with the SAM of TTFP, which appeared the most outstanding performance in conventional OFETs in Chapter 4. The Ph-BTBT-10 OFETs with TTFP-treated solution-processed silver S/D electrodes achieved FET mobility of 0.18 cm^2/Vs. Compared to pristine solution-processed silver electrodes, OFETs performance was improved resulting in two orders of magnitudes in FET mobility increased. Therefore, it could imply that self-assembled monolayer plays a role to enhance the hole injection in the case of printed electrodes also.

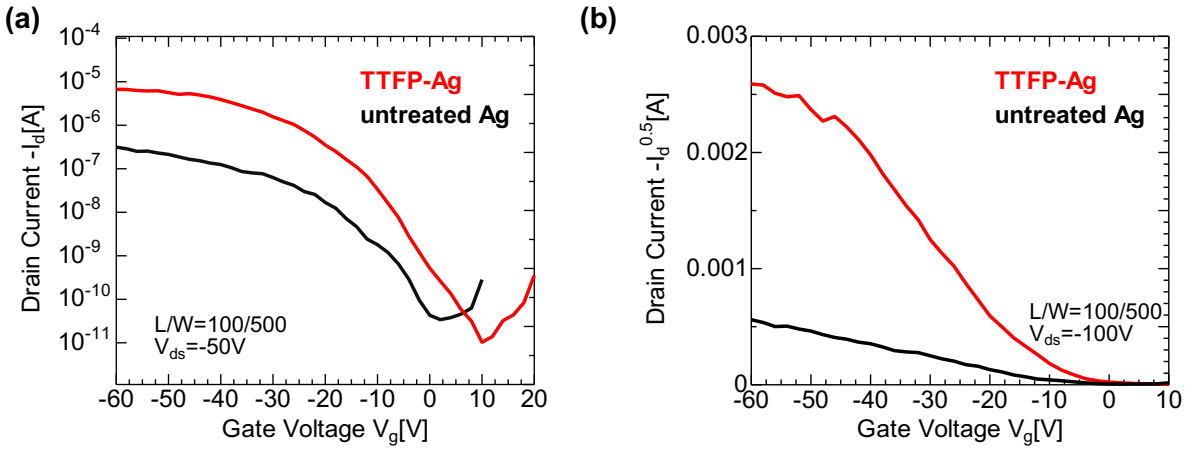

Figure 5.14 Characteristics of OFETs with photo pattering (a) pristine silver electrodes (b) silver electrodes modified with TTFP

5.5 Conclusion and prospective

Various solution-processed silver electrode patterning methods were investigated which is inkjet printing and methos utilizing properties of hydrophobic and hydrophilic based on the differential surface energy with three concepts: the hydrophobic and hydrophilic SAM; CYTOP layer with O_2 plasma; hydrophobic photoreactive SAM. And I could achieve to completed Ph-BTBT-10 thin-film transistors using in photo pattering method, while other methods are still needed further investigation to complete fabrication of OFETs. Although Ph-BTBT-10 thin-film transistors with solution-processed silver S/D electrodes were successfully operated and SAM treatment was effective, compared to those with the vacuum-deposited silver S/D electrodes its properties showed inferior. Thus, discussing the reason and improvement approach is needed. First, the thickness of solution-processed silver S/D electrodes is thick (over several hundred nm), hence, it can affect the morphology of Ph-BTBT-10 layer and injection of the hole. The thickness is determined by the technique of coating, now it has been conducted in person with squeegees, so the next goal is to fabricate solution-processed silver S/D electrodes with the same thickness (about 30 nm) of vacuum deposited silver S/D electrodes.

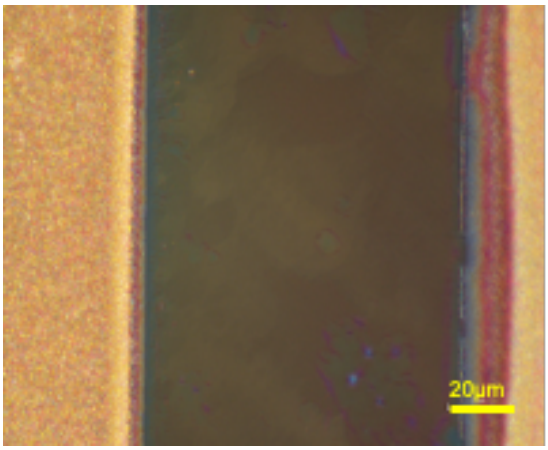

Figure 5.15 Optical images of Ph-BTBT-10 thin film transistor with solution processed silver electrodes patterned by photoreactive self-assembled monolayer.

References

[1] A. Teichler *et al.*, "Combinatorial Screening of Polymer:Fullerene Blends for Organic Solar Cells by Inkjet Printing," *Adv Energy Mater*, vol. 1, no. 1, pp. 105–114, Jan. 2011, doi: 10.1002/AENM.201000027.

[2] H. Minemawari *et al.*, "Inkjet printing of single-crystal films," *Nature*, vol. 475, no. 7356, p. 364, Jul. 2011, doi: 10.1038/nature10313.

[3] M. Gao, L. Li, and Y. Song, "Inkjet printing wearable electronic devices," *J Mater Chem C Mater*, vol. 5, no. 12, pp. 2971–2993, Mar. 2017, doi: 10.1039/C7TC00038C.

[4] R. R. Søndergaard, M. Hösel, and F. C. Krebs, "Roll-to-Roll fabrication of large area functional organic materials," *J Polym Sci B Polym Phys*, vol. 51, no. 1, pp. 16–34, Jan. 2013, doi: 10.1002/POLB.23192.

[5] B. Kang, W. H. Lee, and K. Cho, "Recent advances in organic transistor printing processes," *ACS Appl Mater Interfaces*, vol. 5, no. 7, pp. 2302–2315, Apr. 2013, doi: 10.1021/AM302796Z/ASSET/IMAGES/MEDIUM/AM-2012-02796Z_0014.GIF.

[6] K. Huang *et al.*, "Rapid laser annealing of silver electrodes for printing organic thin-film transistors on plastic substrates," *IEEE Trans Electron Devices*, vol. 66, no. 6, pp. 2729–2734, Jun. 2019, doi: 10.1109/TED.2019.2911310.

[7] G. Kitahara, K. Aoshima, J. Tsutsumi, H. Minemawari, S. Arai, and T. Hasegawa, "Low-voltage operation of organic thin-film transistors based on ultrafine printed silver electrodes," *Org Electron*, vol. 50, pp. 426–428, Nov. 2017, doi: 10.1016/J.ORGEL.2017.08.023.

[8] M. Minagawa, K. Kobayashi, S. Sone, and K. Shinbo, "Improvement of organic field-effect transistor characteristics via oxidation treatment of Ag nano-ink electrode surfaces," *Jpn J Appl Phys*, vol. 59, no. SC, p. SCCA03, Nov. 2019, doi: 10.7567/1347-4065/AB48CB.

[9] R. Sugano, Y. Takeda, Y. Kobayashi, K. Fukuda, D. Kumaki, and S. Tokito, "Fine patterning method for silver nanoparticle electrodes using differential hydrophobic and hydrophilic surface properties," *Jpn J Appl Phys*, vol. 53, no. 4 SPEC. ISSUE, p. 04EK01, Feb. 2014, doi: 10.7567/JJAP.53.04EK01/XML.

[10] S. H. Kim, H. Otsuka, H. W. Shin, K. Tanaka, R. C. Advincula, and H. Usui, "Manipulation of work function and surface free energy of tungsten oxide hole injection layer modified with a self-assembled monolayer," *Jpn J Appl Phys*, vol. 50, no. 1 PART 3, p. 01BB01, Jan. 2011, doi: 10.1143/JJAP.50.01BB01/XML.

[11] C. Liu, Y. Li, M. V. Lee, A. Kumatani, and K. Tsukagoshi, "Self-assembly of semiconductor/insulator interfaces in one-step spin-coating: A versatile approach for organic field-effect transistors," *Physical Chemistry Chemical Physics*, vol. 15, no. 21.

pp. 7917–7933, Jun. 07, 2013. doi: 10.1039/c3cp44715d.

[12] S. H. Kim *et al.*, "High-performance solution-processed triisopropylsilylethynyl pentacene transistors and inverters fabricated by using the selective self-organization technique," *Appl Phys Lett*, vol. 93, no. 11, 2008, doi: 10.1063/1.2987419.

[13] Y. Li, H. Sun, Y. Shi, and K. Tsukagoshi, "Patterning technology for solution-processed organic crystal field-effect transistors," *Science and Technology of Advanced Materials*, vol. 15, no. 2. Institute of Physics Publishing, 2014. doi: 10.1088/1468-6996/15/2/024203.

Chapter 6
Conclusion and prospective

6.1 Summary

Organic field effect transistors (OFETs) have been investigated for many years due to their potential applications in flexible, large-area, and low-cost electronics. 2-Decyl-7-phenyl-[1]benzothieno[3,2-b][1]benzothiophene (Ph-BTBT-10), which is one of the liquid crystalline organic semiconductors, is easy to fabricate uniform films by spin coating technique and the resulting uniform thin films exhibit high mobility even though polycrystalline films. Thus, this material is suitable for practical applications with solution processes. Most reports of Ph-BTBT-10 OFETs used gold source-drain (S/D) electrodes due to their outstanding properties. Unfortunately, the high cost of gold has overshadowed its applications in low-cost electronics. Therefore, it is aimed at fabricating high-performance and low-cost OFETs using Ph-BTBT-10 OFET and silver S/D electrodes.

In Chapter 3, top-contact configuration Ph-BTBT-10 OFETs with silver S/D electrodes were investigated and exhibited intriguing results that the performance of OFETs did not depend on the work function of the metal electrodes, which silver and gold are 4.6 eV and 5.0 eV, respectively. Ph-BTBT-10 OFET with silver S/D electrodes exhibited comparable carrier mobility (8.2 cm^2/Vs) to those with gold S/D electrodes (11.9 cm^2/Vs). For the contact resistance, a value less than 0.5 kΩcm was obtained, which is an order of magnitude lower than OFETs with gold S/D electrodes (2.7 kΩcm). Therefore, the possible reasons why Ph-BTBT-10 OFETs with silver S/D electrodes

perform superior to those with gold S/D electrodes despite the energy level mismatches were discussed. It was assumed that silver electrodes may easily penetrate into the Ph-BTBT-10 semiconductor layer upon the deposition of silver electrodes. So, cross-section analyses were conducted through time-of-flight secondary ion mass spectrometry (TOF-SIMS), scanning electron microscope (SEM), and X-ray reflectometry (XRR) to clarify the mechanism. TOF-SIMS enables us to observe the silver and gold distribution into the Ph-BTBT-10 layer, and there was a significant difference in the distribution of sulfur ions which indicated the existence of Ph-BTBT-10 layer. For silver, the layer that exists only silver electrodes might be very thin, and the mixed layer of silver electrodes and Ph-BTBT-10 could be formed relatively up to the upper position, while gold electrodes appeared thick. It might imply that silver electrodes penetrated Ph-BTBT-10 layer more deeply compared to gold electrodes. This affects decreasing access resistance, which is one of the dominant elements of contact resistance in the bottom-gate top-contact configuration. Based on SEM and XRR results, it was inferred that silver electrodes penetrated into Ph-BTBT-10 layer deeply, since the interface between electrodes and Ph-BTBT-10 layer was very rough while gold electrodes showed a relatively flattened interface. Also, as a result of this larger interface area, the carrier injection area is increased and Ph-BTBT-10 OFET with silver S/D electrodes achieves a small contact resistance.

In Chapter 4, the bottom-contact configuration Ph-BTBT-10 OFETs with silver S/D electrodes were investigated because the bottom-contact structure is feasible for industrial applications such as photolithography and solution processes. However, it suffers from lower performance because the poor contact condition between organic semiconductors and S/D electrodes contributes in large part to the contact resistance. Ph-BTBT-10 OFETs

with silver S/D electrodes showed very low OFET mobility (0.1 cm^2/Vs) and high contact resistance (630 kΩcm) because the work function of silver has a large energy level misalignment with the highest occupied molecular orbital (HOMO) level of Ph-BTBT-10 (-5.6 eV). Therefore, interface engineering is necessary to enhance the charge carrier injection. In this thesis, the modification of the electrode by a self-assembled monolayer (SAM) treatment, which is to play with the energy shift at the metal-semiconductor interface by deliberately introducing an interface dipole, was investigated. The silver S/D electrodes were modified with pentafluorobenzenethiol (PFBT) and tetrafluoro-(trifluoromethyl)-benzenethiol (TTFP), respectively. Ph-BTBT-10 OFETs with SAM-treated silver S/D electrodes achieved mobility of an average of 1.5 cm^2/Vs and the contact resistance two orders of magnitude lower than OFETs with pristine silver S/D electrodes. Also, Ph-BTBT-10 OFETs with TTFP-modified silver S/D electrodes showed deep work function (6.0 eV) and small contact resistance (2.1 kΩcm), it can be expected to utilize a deeper HOMO level of organic semiconductors. Bottom-contact OFET is a practical structure for the application of solution processes since silver nanoparticles can damage the organic layer when electrodes are fabricated in the top-contact structure. Therefore, based on these conventional process results, solution-processed silver S/D electrodes were investigated.

In Chapter 5, solution-processed silver S/D electrodes by using silver nanoparticles were applied to Ph-BTBT-10 OFETs. First, the inkjet printing process which has the advantage of the drop-on-demand method was conducted. Although relatively non-wavy dot line patterns were obtained by adjusting conditions between silver nanoparticles and surfaces, it was difficult to control fabrication conditions and obtain fine patterns. To achieve fine patterns, differential surface properties of hydrophobic and hydrophilic were

utilized. To pattern electrodes, three concepts were investigated: hydrophobic and hydrophilic SAMs, fluorinated polymer (CYTOP) layer with oxygen plasma, and hydrophobic photoreactive SAM. The basic concept is silver nanoparticles can be controlled to be fabricated only on hydrophilic surfaces. After hydrophobic treatment of the underlayer, the designated area for S/D electrodes is conducted in hydrophilic properties, consequently, silver S/D electrodes will be patterned. Fine patterns were achieved through CYTOP layer with oxygen plasma and photoreactive SAM. However, the residue of CYTOP on the channel area impeded the fabrication of Ph-BTBT-10 semiconductor layer due to issues with hydrophobicity and thickness. For photoreactive SAM, the SAM layer is thin, and photoreactive protecting groups of SAM on the channel area can be removed as UV exposed after fabricating silver S/D electrodes, and additional UV/ozone cleaning improved the uniform formation of Ph-BTBT-10 thin film. As a result, Ph-BTBT-10 OFETs with solution-processed silver S/D electrodes were successfully fabricated and operated. Ph-BTBT-10 OFETs with TTFP-treated silver S/D electrodes by fabricating solution process showed the mobility of 0.18 cm^2/Vs.

Ph-BTBT-10 OFETs with silver S/D electrodes showed meaningful results as next-generation organic electronics: superior performance to OFETs with gold S/D electrodes in the top contact configuration; the possibility of utilization for display, showing the mobility of over 1 cm^2/Vs in the bottom contact configuration with SAM. Furthermore, this approach is also expected to realize an ultra-low-cost all-solution process. These results envision that Ph-BTBT-10 OFET with silver S/D electrodes is a promising candidate.

6.3 Future prospective

In this study, liquid crystalline organic semiconductor Ph-BTBT-10 OFETs with silver S/D electrodes were realized showing outstanding performance in both the top-contact and bottom-contact configurations and were demonstrated possible reasons. Also, Ph-BTBT-10 OFETs with solution-processed silver S/D electrodes were successfully fabricated. However, there are several issues that require further investigation.

1) The concept of the CYTOP layer using oxygen plasma also remains a good candidate for fine patterning. Current status, it is hard to form Ph-BTBT-10 thin film onto the CYTOP layer due to its thickness or hydrophobic properties. Therefore, it is the key task to control the residue of CYTOP in the channel area. By applying O_2 plasma on the channel area after fabrication of silver S/D electrodes, the CYTOP layer can be removed, however, it sometimes damages silver S/D electrodes, so the reproducibility was unstable. Therefore, the etching method by immersing the devices in the solvent of CYTOP has been considered. However, this process takes a considerable amount of time, so combining immersing etching and dry etching can be considered. After immersing the device in the solvent of CYTOP and applying a short-term O_2 plasma, it is expected to minimize the damage to silver S/D electrodes while maintaining the fabrication of finely etched patterns.
2) Even though Ph-BTBT-10 OFETs with solution-processed silver S/D electrodes were successfully fabricated, compared to those with the vacuum-deposited silver S/D electrodes the properties need to be improved. The thickness of solution-processed silver S/D electrodes is thick (hundreds of nanometers), hence, it can affect the morphology of Ph-BTBT-10 layer and injection of the hole. As mentioned in Chapter 4, charge carrier injection from the side of electrodes greatly affects when the thickness of electrodes is

thinner, but too thick electrodes can suppress the injection from the top of electrodes. Moreover, it can cause the misalignment of Ph-BTBT-10 molecules in the boundary between S/D electrodes and organic semiconductors. Therefore, it is required to compare OFETs with solution-processed silver S/D electrodes at the same thickness as those with vacuum-deposited silver S/D electrodes. The investigation of the relation between OFET performance and the thickness of solution-processed S/D electrodes is also meaningful. According to Nikon Corporation, blade coating with squeegees can achieve thin electrodes, a thickness is tens of nanometers. However, this greatly depends on the technique of the experimenter so further investigation is expected.

Publications

Publications

- Sabina Kang, Jun-ichi Hanna, and Hiroaki Iino, “High-performance organic field effect transistor of liquid crystalline organic semiconductor using silver electrodes with bottom-gate top-contact configuration”, *Applied Physics Express*, 2023, 16.9: 091005. (Chapter 3)
- Sabina Kang, Jun-ichi Hanna, and Hiroaki Iino, “Interface engineering to enhance charge injection in Ph-BTBT-10 organic semiconductor thin film transistor with silver source-drain electrodes.” *Molecular Crystals and Liquid Crystals*, 2023, 1-8 (Chapter 4)

International Conferences

- Sabina Kang, Jun-ichi Hanna, and Hiroaki Iino, “Interface engineering to enhance charge injection in Ph-BTBT-10 organic semiconductor thin film transistor with silver source-drain electrodes” KJF International Conference on Organic Materials for Electronics and Photonics 2022, Jeju, Korea.
- Sabina Kang, Jun-ichi Hanna, and Hiroaki Iino, “High-performance low-cost OFETs with silver electrodes on organic semiconductor Ph-BTBT-10 in top contact geometry,” The 10th International Conference on Molecular Electronics and Bioelectronics 2019, Nara, Japan.

Domestic Conferences

- Sabina Kang, Jun-ichi Hanna, and Hiroaki Iino, “Effects of Silver Source-Derain Electrodes on Liquid Crystalline Organic semiconductor and its OFET performance,” The 66th Japan Society of Applied Physics Spring Meeting 2019, Tokyo, Japan.